Journal of the Geological Survey of Brazil

Petrography, geochemistry and zircon U-Pb geochronology of the Siderian-Rhyacian granitoids of NW Bacajá Domain, Amazonian Craton

Cleberson da Silva Vieira[a]; Wagner da Silva Amaral[a]; Felipe Holanda dos Santos,[b,*]

[a]Institute of Geosciences, University of Campinas (UNICAMP), Rua Carlos Gomes, Campinas, SP, Brazil, CEP: 13083-855
[b]Institute of Geosciences and Engineering, Federal University of Western Pará (UFOPA), Rua Vera Paz, Santarém, PA, Brazil, CEP: 68040-255

Abstract

Archean and Paleoproterozoic granitoids with different geochemical affinities are widely distributed in the basement of high-grade metamorphic rocks of the Bacajá Domain, which consists of Rhyacian granite-greenstone terrain with Archean-Siderian fragments, one of which is in the southeastern Amazonian Craton. Understanding the diversity of these rocks in the geological record is essential to improve the evolution of knowledge of the Amazonian Craton. Thus, this work presents petrographic, geochemical, and geochronological (U-Pb LA-ICP-MS in zircon) data on granitoids of the São José Complex, Canaã Granite, Sant'Ana Granodiorite and Uirapuru Granite, that occur in the northwestern of the Bacajá Domain. São José Complex is composed of biotite tonalites and granodiorites slightly peraluminous from medium to high-K, magnesian and I-type affinities. One U-Pb zircon age was obtained at 2502 ± 6 Ma, which may represent a subduction magmatism in pre-collisional stage arc environment prior to the Transamazonian Orogeny, formed from the melt of Archean crustal sources and amphibolitic rocks. The granitoids like Canaã Granite, Sant'Ana Granodiorite and Uirapuru Granite are composed of weakly metaluminous to peraluminous monzogranites, granodiorites with subordinate tonalites and syenogranites, with high SiO_2 and K_2O contents and high-K calc-alkaline to shoshonitic affinities, of ferroan I-type and A-type. The age of 2124 ± 7 Ma was obtained for the Sant'Ana Granodiorite, which may indicate its formation in syn- to post-collisional environments related to magmatic episodes of the Transamazonian Orogeny. The granodiorite was crystallized from partial melt of crustal sources derived from intermediate rocks such as tonalites and psammitic gneisses that occur in the region.

Article Information

Publication type: Research Papers
Received 21 March 2022
Accepted 26 August 2022
Online pub. 9 September 2022
Editor: J.M. Lafon

Keywords:
Granitoids;
Petrogenesis;
U-Pb geochronology;
Transamazonian orogeny

*Corresponding author
Felipe Holanda dos Santos
felipeholanda@ige.unicamp.br

1. Introduction

The Paleoproterozoic was an era of significant tectonic, climatic, and biological upheavals in the Earth system (Gumsley et al. 2017). Among the tectonic modifications, it is possible to mention decreases (2.42-2.22 Ga) and increases (1.9 Ga) in superplumes activities (Condie 2000, 2009a,b) and the first appearance of accretionary and collisional orogens (Corrigan et al. 2009). Furthermore, one of the best-preserved examples of Paleoproterozoic high-pressure rocks in the Trans-Hudson Orogen indicates one of the first operations of tectonic plates, similar to those from the Phanerozoic regime (Weller and St-Onge 2017). The early history of the supercontinent cycle also dates back from the Paleoproterozoic, where the amalgamation and dispersion of the Nuna supercontinent take place between 1.9 and 1.8 Ga (Zhao et al. 2002; Reddy and Evans 2009). The Archean-Proterozoic transition also marks secular changes in the magmatic record. The melting of a subducting plate dominated the generation of magmatic rocks in the Neoarchean, whereas in the early Paleoproterozoic, the partial melting of the metasomatized mantle wedge was the primary process to produce magma in the crust (Wyllie 1983; Hawkesworth et al. 1993; Kemp and Hawkesworth 2003; Martin et al. 2005).

The secular changes in the magmatic record during the Paleoproterozoic indicate the predominance of lithological associations constituted by tonalite, granodiorite, and andesite with calc-alkaline signatures (Baker et al. 1981), in opposition to the Archean associations dominated by the tonalitic-trondhjemitic-granodioritic rocks – TTG (Martin 1994; Martin and Moyen 2002; Martin et al. 2005). For more than a decade, it was recognized that the period from 2.5 to 2.2 Ga (Siderian-

ISSN: 2595-1939
https://doi.org/10.29396/jgsb.2022.v5.n3.1
Open access at jgsb.cprm.gov.br

Rhyacian) had marked by an apparent "global magmatic shutdown," interpreted as a consequence of changes in the tectonic plate regime (Condie et al. 2005; Condie et al. 2009b) . This time was known as Siderian Quiet Interval – SQI (Condie et al. 2005; Condie et al. 2009b). However, several authors have identified magmatic rocks of age coincident with SQI in different regions of the globe (e.g., Gawler Craton, Dharwar Craton, Borborema Province, Amazonian Craton), including juvenile magmatic records of TTG arc-like signatures, supporting significant crustal additions in the Siderian within the cratons (Swain et al. 2005; Berman et al. 2005; Vasquez et al. 2008; Santos et al. 2009; Anderson et al. 2012; Santosh et al. 2013; Pehrsson et al. 2014).

Several orogenic systems formed by terrane accretion along subduction zones are recognized in the Rhyacian period, constituting granite-greenstone terrains (e.g., Zhao et al. 2002; Brito Neves 2011; Brito Neves and Fuck 2014). The Rhyacian chrono-correlates orogenic events receive various names in different regions of the world, such as Transamazonian Orogeny (Hurley et al. 1967; Almeida et al. 1973) in the South American Continent; Eburnian Orogeny (Bessoles 1977; Liegeois et al. 1991) and Birimian Orogeny (Milési et al. 1992; Grenholm 2019; Grenholm et al. 2019) in Africa.

In the Amazonian Craton, Paleoproterozoic rocks from the Siderian (2.50-2.30 Ga) and Rhyacian periods (2.30-2.05 Ga) are included in the Maroni-Itacaiúnas or Transamazonian Province, a region consisting of granite-greenstone terrains generated and/or reworked during the Transamazonian Cycle (2.25-2.00 Ga) (Cordani et al. 1979; Tassinari and Macambira 1999; Santos et al. 2000; Santos 2003; Santos et al. 2006). In the context of the Transamazonian Province, the Bacajá Domain located to the south of this province, is composed by Archean-Siderian remnants reworked in the Transamazonian Cycle and several granitoids with Rhyacian-Orosirian ages (Vasquez et al. 2008). In the northwestern of Bacajá Domain, several granitoids have been mapped over the past decades, including monzogranites, tonalites, granodiorites, and charnockitic rocks (Macambira et al. 2003; Santos 2003; Vasquez et al. 2005; Vasquez et al. 2008; Barros et al. 2016). These rocks generally occur as intrusive plutons in Archean and Paleoproterozoic high-grade orthogneisses and meta-sedimentary rocks (e.g., Rio Preto Mafic Orthogranulite, Uruará Orthogneiss, and Ipiaçava Paragneiss).

According to Vasquez et al. (2008), the granitoids from the Bacajá Domain have ages ranging from Neo-Archean to Orosirian, are related to collisional and accretionary phases of an expressive Rhyacian orogen, and also may have been produced by the melting of the Archean-Siderian continental crust. Furthermore, the origin of these rocks can be key to unravel the Paleoproterozoic evolution of the Bacajá Domain. The geodynamic significance of the Archean-Paleoproterozoic transition is poorly understood in the region, and therefore, this work aims to characterize these granitoids of the Bacajá Domain, to define their geochemical signatures, magmatic series, geodynamic typologies, and tectonic settings, in addition to investigating and discussing the origin and evolution of magmatic events that make up the northwestern region of the Bacajá. For this, new field, petrographical, geochemical and geochronological (U-Pb method in zircon) data are presented.

2. Geological context

The Bacajá Domain is part of the Maroni-Itacaiúnas or Transamazonian Province (Cordani et al. 1979; Teixeira et al. 1989; Santos 2003) in the east-central region of the Pará State. It consists of rocks representing reworked Archean and Siderian domains from different phases of the Transamazonian Cycle (Santos 2003; Tassinari and Macambira 1999, 2004; Vasquez et al. 2006; Vasquez et al. 2008). The geological evolution of the Bacajá Domain is divided into three main events, including 3.00 – 2.50 Ga Archean magmatism, early-Siderian and late-Siderian metavolcanic-sedimentary sequences (2.50 – 2.34 Ga), and Rhyacian magmatism (2.30 – 2.06 Ga) (Vasquez et al. 2006; Vasquez et al. 2008).

The Neoarchean magmatism is represented by orthogneisses with crystallization ages ranging from 2671 to 2503 Ma with positive εNd (+2,67), indicating the formation of juvenile Archean crust (Macambira et al. 2004). The Early-Siderian event is constituted by felsic metavolcanic rocks and meta-quartz diorites from 2452 to 2440 Ma, hosted in Rhyacian granitoids related to island arc settings associated with a Neoarchean nucleus (Vasquez et al. 2008). The Três Palmeiras greenstone belt (Macambira et al. 2004) is related to meta-tonalites from 2338 Ma island arcs, and ocean floor rocks (Jorge João et al. 1987; Vasquez et al. 2008) and is the main representative sequence from the late-Siderian event. The Rhyacian magmatism is formed by distinct events related to Rhyacian orogenesis. The oldest Rhyacian rocks comprise granitoids of 2313 Ma (Faraco et al. 2005), associated with ortho-granulites and charnockites related to the amalgamation of an island arc against an Archean/early-Siderian block (Vasquez et al. 2008).

Subsequently, in the Rhyacian, high-temperature deformed granitoids from 2.21 to 2.18 Ga are related to an early-Rhyacian orogeny formed in a continental magmatic arc setting, installed on the margin from a Neoarchean to Siderian microcontinent (Vasquez et al. 2008). Syn-collisional orogenic granitoids from 2.16 to 2.13 Ga related to a magmatic arc (Macambira et al. 2003; Vasquez et al. 2005) and late-collisional to post-collisional granites from 2.11 to 2.09 Ga and charnockitic rocks with low deformation (Vasquez et al. 2008) also occur. The youngest Rhyacian rocks comprise post-collisional charnockite granites from 2.08 to 2.07 Ga related to the post-collisional stage of the Transamazonian Orogeny (Macambira et al. 2003; Souza et al. 2003; Vasquez et al. 2005; Vasquez et al. 2008). A later magmatic episode of Orosirian age, dated at 1.99 Ga, occur locally in the northwestern of the Bacajá Domain. This magmatism is composed by granitic rocks intruded in high-grade metamorphic rocks and Rhyacian granitoids. The 1.99 Ga granitoids may represent a late magmatic pulse of the Transamazonian Cycle or may be part of the Orosirian orogenic magmatism associated with the Tapajós-Parima Province (Vasquez et al. 2005). According to Vasquez and Rosa-Costa (2008), the main units composed of granitic rocks from the northwestern region of the Bacajá Domain (Figure 1) are represented by the Canaã Granite, Arapari Intrusive Suite, and by the Sant'Ana Granodiorite. These lithological associations represent syn- to post-collisional stages of the Transamazonian Orogenesis and intruded the Archean-Paleoproterozoic basement constituted by the Ipiaçava Paragneiss, Uruará Orthogneiss and Rio Preto Mafic Orthogranulite.

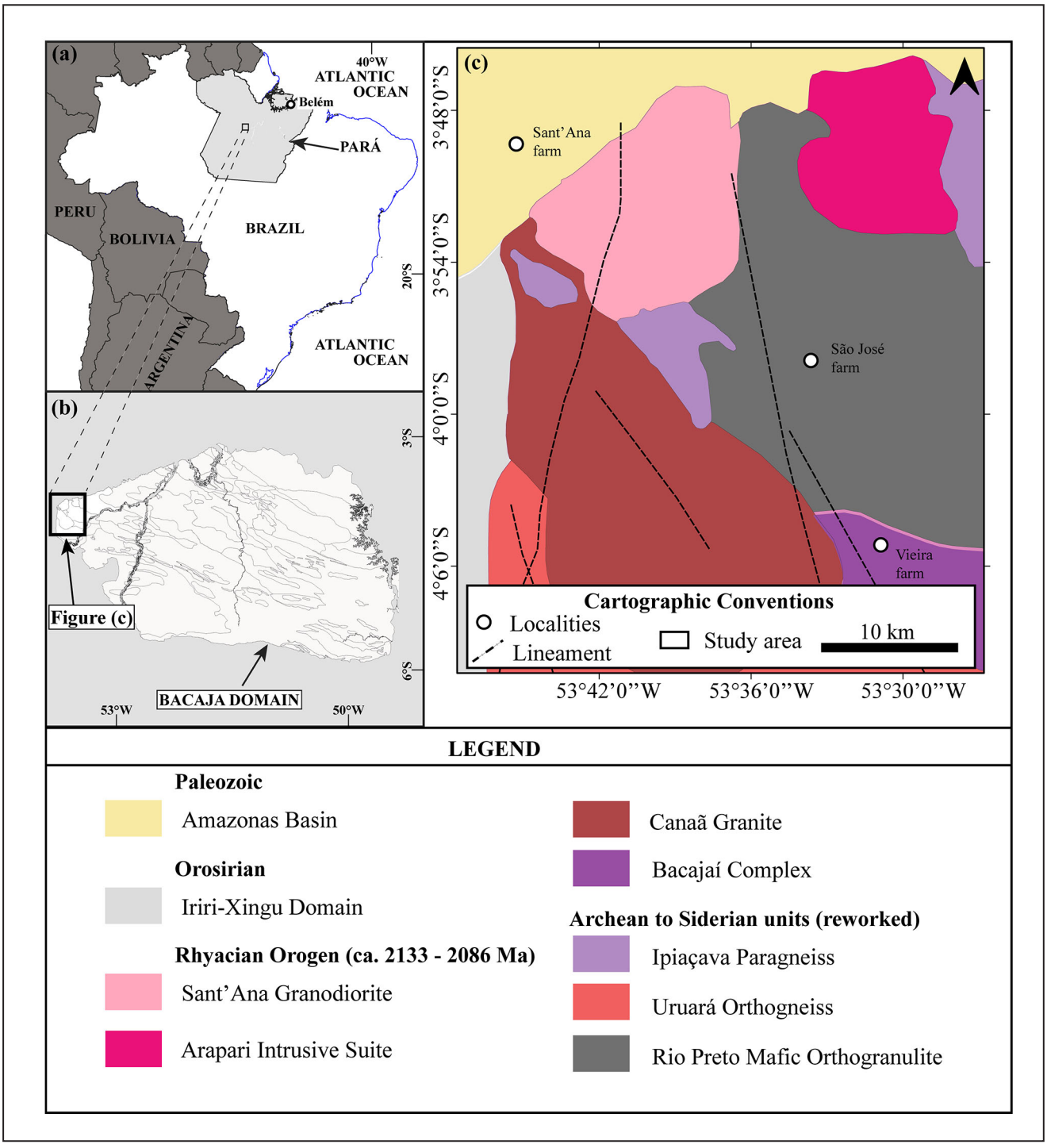

FIGURE 1 – Location map of the study area (a-b) Location of the Bacajá Domain in the context of South America; (c) Geological map of the study region in the Bacajá Domain by Vasquez and Rosa-Costa (2008) – Data source: SGB/CPRM (https://geosgb.cprm.gov.br/downloads/#).

The Rio Preto Mafic Orthogranulite occurs as elongated bodies within a WNW-ESE trend. It consists of two pyroxenes mafic rocks and migmatitic orthogneisses, representing a probable exhumed lower crust (Jorge João and Silva Neto 1994; Vasquez et al. 2008). Zircon Pb-evaporation geochronological data for a tonalitic granulite yielded an age of 2628 ± 3 Ma, interpreted as the timing of protolith crystallization (Vasquez 2006; Vasquez and Rosa-Costa 2008). These authors believed that metamorphism in granulite facies took place at 2072 ± 3 Ma. The Uruará Orthogneiss is constituted of layered metatonalites and metagranodiorites, which locally exhibit migmatitic features and amphibolitic lenses (Vasquez et al. 2005). SHRIMP zircon U-Pb geochronological data indicate crystallization ages of 2503 ± 10 Ma for the metatonalite protolith (Santos 2003), whereas Vasquez et al. (2008) present a crystallization age of 2481 ± 13 Ma for one metagranodiorite. The Ipiaçava Paragneiss comprises foliated rocks within an NW-SE trend, consisting of pelitic and psammitic paragneiss metamorphosed into upper amphibolite to granulite facies (Vasquez et al. 2005; Vasquez 2006; Vasquez et al. 2008). The detrital zircon spectra for these meta-sedimentary rocks yielded older populations ranging from 3.12 to 2.56

Ga, whereas monazite crystals extracted from a granitic leucossome showed U-Pb ages between 2074 ± 3 and 2071 ± 3 Ma (Vasquez 2006).

The Canaã Granite is an NNW-SSE oriented pluton, intrusive in the Uruará Orthogneiss, Ipiaçava Paragneiss and Rio Preto Mafic Granulite. It consists of biotite-rich monzogranites and granodiorites (Vasquez et al. 2005; Vasquez et al. 2008). The geochronological data show crystallization ages by the Pb-evaporation method in zircon at ca. of 2104 ± 5 Ma of a monzogranite from the Canaã Granite (Vasquez et al. 2005). This unit is considered representative of the syn-collisional magmatism from the Transamazonian Orogeny. The Arapari Intrusive Suite is formed by charnockitic and charno-enderbitic batholiths and/or stocks, isotropic to slightly foliated with red biotite and hornblende (Ricci 2006). A jotunite and charno-enderbite from this unit were dated by the zircon Pb-evaporation method and yielded crystallization ages ranging between 2070 ± 3 and 2077 ± 3 Ma (Santos 2003; Vasquez et al. 2008). Zircon U-Pb analyses by SHRIMP yielded an age of 2086 ± 5 Ma from a charnockite (Santos 2003) of this suite, which was related to a syn- to late-collisional magmatism phase of the Transamazonian Cycle (Vasquez et al. 2008). The Sant'Ana Granodiorite is formed by a pluton intrusive in the Rio Preto Mafic Orthogranulite and the Ipiaçava Paragneiss, and it consists mainly from medium to fine isotropic, inequigranular granodiorites, and tonalites with an incipient magmatic foliation (Vasquez et al. 2005; Vasquez et al. 2008). Usually, the Sant'Ana Granodiorite exhibit recrystallized biotite, epidote, hornblende, and allanite aggregates, besides host enclaves of dioritic dykes showing magma mingling features (Vasquez et al. 2008; Vasquez and Rosa-Costa 2008). The Sant'Ana Granodiorite has a Pb-evaporation age in zircon of 1986 ± 5 Ma (Vasquez et al. 2005), and may represent the last stage of the post-collisional magmatic event of the Transamazonian Cycle, or an event in an anorogenic environment (Vasquez et al. 2005; Vasquez et al. 2008). A summary with crystallization ages of granitoids from the Bacajá Domain is showed in Table 1.

3. Material and methods

3.1. Geological Mapping and Petrography

The fieldwork was carried out in the Uruará – PA region and allowed to recognize, map and sample the lithological units for petrographic, geochemical, and geochronological studies. The collected data were integrated, resulting in a geological map of the region under study. The petrographic description of the granitoids consisted of identifying the mineralogy, description of magmatic, post-magmatic and alteration textures, modal compositions, and classification according to IUGS definition (Streckeisen 1976; Le Maitre et al. 2002). The mineral abbreviation names followed the systematic proposed by Whitney and Evans (2010).

3.2. Whole-Rock Geochemistry

Whole-rock geochemical analyses were carried out in 14 samples: São José Tonalite (4), Canaã Granite (3), Sant'Ana Granodiorite (4), and Uirapuru Porphyritic Granite (3). Major and trace element analyses were performed by X-ray fluorescence (XRF) at the Geochemistry Laboratory of the Institute of Geosciences (IG-UNICAMP), using a Phillips PW 2404 X-ray fluorescence spectrometer and following the procedures described in Vendemiatto and Enzweiler (2001). Pressed pellets from powder samples were prepared by mixing 9g of the sample with 1.5 g of powdered wax using a hydraulic press (HTP 40, Herzog). Glass discs were made by melting at 1000°C 6g of sample powder mixed with 1g of lithium tetraborate and metaborate. The analytical accuracy of X-ray fluorescence analyses for major oxides and minor elements ranges from 1.5% (SiO_2) to 7% (P_2O_5), while those of trace elements range from 3 to 10%, all with a range of 95% confidence.

Additional analyses of trace elements, including rare earth elements, was performed by inductively coupled plasma mass spectrometry (ICP-MS) at the Isotopic Geology Laboratory of the IG-UNICAMP. The equipment used was an ICP-MS Xseries II (Thermo), equipped with CTT (Collision Cell Technology). For quality control, the GS-N reference (Granite – ANRT) was used. The sample preparation for analysis of trace elements and rare earth elements is described below: The powder samples were dissolved in nitric acid (HNO_3) and hydrofluoric acid (HF) using closed vessels inserted and heated to high pressures and temperatures for approximately five days. After cooling to room temperature, the samples were heated on a hot plate with 0.5 mL of $HClO_4$ for 4 hours at 150°C, to decompose the fluorides. Quality control was performed by analyzing international reference materials (JGb-1, BRP-1), sample duplicates, and a blank sample. The geochemical analyses were plotted using the GCDkit software (Janousek et al. 2006).

3.3. Zircon U-Pb Geochronology

The sample preparation was performed as follow: (1) reduction of the fraction collected using a jaw crusher; (2) pulverizing in a disc mill; (3) concentration of dense minerals in a manual pan; (4) separation of magnetic minerals; (5) separation of the zircon grains in a binocular magnifying glass; (6) mounting the crystals within an epoxy resin and polishing with diamond paste to expose the inner portions of the zircon crystals.

Recognition of the internal structure of zircon crystals was obtained by cathodoluminescence (CL) and backscattered electrons (BSE) in a Cartl Zeiss scanning electron microscope (SEM) with a LEO 430i energy dispersive X-ray microanalyzer. The images helped choose the spots to be dated, by identifying the rim and core, zoning, and fractures present in the zircon. The U–Pb analyses were performed using the LA-SF-ICP-MS technique, which is composed of a Photon Machines Excite.193 ionization laser system equipped with two HelEx cells was used in conjunction with a ThermoScientific Element XR ICP-MS, of the Laboratory of Isotopic Geology at UNICAMP. Helium was used as transporting gas, in order to increase the transport efficiency of the ionized material. The analyses were performed based on the procedures defined by Navarro et al. (2015) with a laser spot size of 25 µm. Data reduction was done using the Iolite software, and the concordia and discordia diagrams was performed using the IsoPlotR software (Vermeesch 2018). All measurements were normalized in relation to the standard zircon 91,500 (Wiedenbeck et al. 1995). Peixe zircon standard (ID-TIMS age of 564 ± Ma; cf. Dickinson and Gehrels 2003) was used to monitor the quality of the reduction procedures.

TABLE 1 - Crystallization ages of granitoids from the Bacajá Domain

Magmatic episode	Geological unit	Age (Ma)	Method	Reference
Post-orogenic magmatism	Sant'ana Granodiorite	1986 ± 5	Pb-Pb TIMS, zircon	Vasquez and Rosa-Costa (2008)
		2483 ± 11		Vasquez and Rosa-Costa (2008)
		2086 ± 5		Vasquez and Rosa-Costa (2008)
Late- to post-collisional magmatism	João Jorge Intrusive Suite	2076 ± 2	Pb-Pb TIMS, zircon	Macambira et al.. (2003)
		2077 ± 2		Vasquez et al. (2008)
		2097 ± 7		Vasquez et al. (2005)
		2115 ± 9		Vasquez et al. (2005)
	Arapari Intrusive Suite	2219 ± 3	Pb-Pb TIMS, zircon	Vasquez et al. (2005)
		2070 ± 3		Vasquez et al. (2008)
		2077 ± 3		Macambira et al. (2009)
		2079 ± 3		Monteiro (2006)
		2824 ± 22		Monteiro (2006)
		2613 ± 8		Monteiro (2006)
		2415 ± 10		Monteiro (2006)
		2157 ± 3		Monteiro (2006)
		2086 ± 5	U-Pb SHRIMP, zircon	Santos (2003)
		2086 ± 5	U-Pb SHRIMP, zircon	Macambira et al. (2003)
Syn- to late-collisional magmatism	Babaquara Granodiorite	2102 ± 3	Pb-Pb TIMS, zircon	Vasquez (2006)
	Canãa Granite	2104 ± 5	Pb-Pb TIMS, zircon	Vasquez et al. (2005)
		2121 ± 5		Vasquez et al. (2005)
		2139 ± 5		Vasquez et al. (2005)
		2156 ± 7		Vasquez et al. (2005)
	Bacajaí Complex	2094 ± 4	Pb-Pb TIMS, zircon	Monteiro (2006)
		2084 ± 2		Monteiro (2006)
		2108 ± 5		Monteiro (2006)
		2436 ± 3		Monteiro (2006)
		2113 ± 3	U-Pb SHRIMP, zircon	Faraco et al. (2005)
		2113 ± 35		Faraco et al. (2005)
		2673 ± 2		Faraco et al. (2005)
		2114 ± 3	Pb-Pb TIMS, zircon	Monteiro (2006)
		2573 ± 2		Monteiro (2006)
Pre-collisional magmatism	Metatonalite Tapiranga	2133 ± 10	Pb-Pb TIMS, zircon	Souza et al. (2003)
	Piranhaquara Monzogranite	2147 ± 5	U-Pb SHRIMP, zircon	Vasquez et al. (2008)
	Belo Monte Granodiorite	2154 ± 2	Pb-Pb TIMS, zircon	Macambira et al. (2009)
	Oca Granodiortie	2160 ± 3	U-Pb SHRIMP, zircon	Vasquez et al. (2008)
	Rhyacian granitoids	2191 ± 2	U-Pb SHRIMP, zircon	Macambira et al. (2009)
	Brasil Novo Tonalite	2182 ± 6	U-Pb SHRIMP, zircon	Macambira et al. (2007)
		2215 ± 2	Pb-Pb TIMS, zircon	Vasquez et al. (2005
		2182 ± 6	U-Pb SHRIMP, zircon	Santos (2003)
		2209 ± 2	Pb-Pb TIMS, zircon	Vasquez and Rosa-Costa (2008)
		2524 ± 5		Vasquez et al. (2005)
	Quartzmonzodiorite enclave	2440 ± 7	Pb-Pb TIMS, zircon	Vasquez et al. (2005)
Paleoproterozoic greenstone belts	Três Palmeiras greenstone belt	2452 ± 3	Pb-Pb TIMS, zircon	Vasquez (2006)
		2359 ± 2	U-Pb SHRIMP, zircon	Macambira et al. (2004)
Granitic-gnaissic-migmatic association	Rio Bacajá Metatonalite	2313 ± 9	U-Pb SHRIMP, zircon	Faraco et al. (2005)
		2338 ± 5		Vasquez and Rosa-Costa (2008)
	Uruará Orthogneiss	2440 ± 7	Pb-Pb TIMS, zircon	Vasquez et al. (2005)
		2487 ± 13	U-Pb SHRIMP, zircon	Vasquez et al. (2008)
		2581 ± 6		Santos (2003)
		2521 ± 14		Vasquez et al. (2008)
		2548 ± 6		Vasquez et al. (2008)
		2503 ± 10		Santos (2003)
		2581 ± 6		Santos (2003)
	Pacajá Orthogneiss	2671 ± 3	U-Pb SHRIMP, zircon	Macambira et al. (2004)
Archean metamorphic complexes	Aruanã Complex	2606 ± 4	Pb-Pb TIMS, zircon	Vasquez and Rosa-Costa (2008)
	Rio Preto mafic Orthogranulite	2628 ± 3	Pb-Pb TIMS, zircon	Vasquez and Rosa-Costa (2008)
	Novolândia Granulite	2766 ± 70	LA-ICP-MS, zircon	Vasquez and Rosa-Costa (2008)
	Cajazeiras Complex	3009 ± 27	U-Pb SHRIMP, zircon	Macambira et al. (2007)
		2942 ± 4	Pb-Pb TIMS, zircon	Vasquez and Rosa-Costa (2008)
		2057 ± 7	U-Pb SHRIMP, zircon	Macambira et al. (2003)

4. Results

4.1. Field geology and petrography

Although the identification of metamorphic rocks in the field have been done, only the granitic rocks for this work has been discussed. A geological map was made after field, remote sensing, and geophysical data (Figure 2), showing the lithological units from the mapped area. The lithostratigraphic units investigated in this study follow the model proposed by Vasquez and Rosa-Costa (2008). However, the rocks that did not fit within this classification scheme were named in the present work. The contacts among the were inferred mainly through remote sensing and geophysical data (e.g., satellite imagery such as Sentinel 2, Landsat-8, Alos Palsar, and aero geophysical data from gamma spectrometry and magnetometry) as they are difficult to visualize due to the dense vegetation cover and the limited access to specific regions further away from the roads. The geological map also shows the geochemical and geochronological sampling points.

The petrographic characterization was performed on 14 samples of the granitic units (São José Complex, Canaã Granite, Sant'Ana Granodiorite and Uirapuru Granite). The rocks were classified according to Streckeisen (1976) and the modal results were plotted on the QAP and Q-A+P-M' diagrams (Figure 3) and presented in Table 1.

4.1.1. São José Complex

The São José Complex (Figure 4a) consists predominantly of biotite tonalite, biotite granodiorite, and subordinate biotite granites with foliation marked by the alignment of biotite and plagioclase phenocrysts (Figure 4c). In this unit, there are metric amphibolite xenoliths (Figure 4a), lenses of banded iron formation, mafic enclaves composed of biotite, and usually, the rocks are cut by granitic aplitic dykes (Figure 4b).

The tonalite is composed of quartz (30-38%), plagioclase (43-54%), K-feldspar (2-5%) and biotite (13-25%) and the granodiorite consists of quartz (35%), plagioclase (29%), K-feldspar (11%), and biotite (11%). Zircon, apatite, and opaques occur as accessory minerals, while sericite, muscovite, and chlorite occur as secondary minerals. Plagioclase occurs as subhedral crystals (0.5-1.8 mm), exhibits polysynthetic twins, and can be found substituted by sericite (Figure 4d-e). Locally, it presents quartz inclusions in poikilitic texture. Plagioclase also occurs as prismatic (Figure 4f) and/or rounded phenocrysts, larger than 2.5 mm, and is cut by micro faults and microfractures. Its twins exhibit lens-shaped deformation. Quartz occurs as prismatic subhedral crystals (Figure 4d), exhibits undulose extinction, and is sometimes recrystallized in subgrains. Additionally, it also occurs as irregular-shaped interstitial crystals (Figure 4e-f) between plagioclase and biotite. Biotite forms lamellae of medium grain (~1.5 mm) aligned according to the foliation (Figure 4d) and also occurs as tiny crystals (0.2-0.5 mm; Figure 4f). The latter type appears on the margins of plagioclase crystals. Biotite usually contains zircon and apatite inclusions. In more deformed domains, biotite form features such as kink-bands and mica-fish (Figure 4e). Zircon forms small euhedral crystals with pleochroic halos, usually embedded in biotite. Apatite occurs as rounded and/or rod-shaped euhedral crystals usually included in plagioclase. Opaque minerals form subhedral to anhedral crystals usually associated with biotite.

4.1.2. Canaã Granite

The Canaã Granite comprises medium to coarse biotite monzogranite, biotite granodiorite, and biotite tonalite. They are isotropic to weakly foliated, with foliation marked by biotite alignment (Figure 5a). Xenoliths are found in this unit. Most of them are angular fragments with approximately 5 to 10 cm formed by biotite gneisses (Figure 5b). The monzogranite (Figure 5c) is essentially composed of quartz (32-34%), plagioclase (36-37%), K-feldspar (24-27%), and biotite (~3-4%), and the granodiorite is composed of quartz (33%), plagioclase (30%), K-feldspar (32%) and biotite (2%); while tonalite presents quartz (38%), plagioclase (54%), K-feldspar (2%), and biotite (3%). Zircon, apatite, allanite, garnet, and opaques occur as accessory minerals, while sericite, muscovite, and chlorite occur as secondary minerals. Garnet occurs locally and rarely appears in monzogranite of more felsic composition.

In these lithotypes, plagioclase occurs as crystals greater than 5 mm, they are rounded (Figure 5d) and sometimes have microfractures filled with quartz and biotite, in addition to deformational features such as folded twin planes. Plagioclase also appears as medium (0.8-2.5 mm) subhedral and anhedral crystals, with polysynthetic twins, and is usually replaced by sericite (Figure 5e). K-feldspar occurs as prismatic crystals (>5 mm), usually exhibiting chessboard twins and/or perthites of variable morphologies (Figure 5d); There are also euhedral to subhedral crystals (2-4 mm) that show chessboard twins, and their contacts are usually bordered by fine quartz and biotite crystals. Locally, zircon and plagioclase inclusions occur in K-feldspar. Quartz occurs as a medium to coarse (0.7-2.0 mm) subhedral crystals with undulose extinction (Figure 5d-e) or recrystallized interstitial crystals forming subgrains (Figure 5e). Additionally, crystals with vermiform shapes also occur among the boundaries of the feldspar crystals, defining a myrmekite texture (Figure 5d). Biotite forms subhedral to anhedral tabular crystals (0.2-1.5 mm) (Figure 5d), besides clusters distributed along with quartz. Sometimes biotite is partially replaced by chlorite and muscovite and exhibits inclusions of tiny apatite, allanite, and zircon crystals. Garnet forms fractured fine to medium subhedral and anhedral crystals (0.3-2.5 mm) (Figure 5f), usually associated with biotite.

4.1.3. Sant'Ana Granodiorite

The Sant'Ana Granodiorite (Figure 6a-b) is predominantly composed of biotite granodiorites and biotite monzogranites and subordinate tonalites. The granodiorite (Figure 6b) consists of quartz (28-35%), plagioclase (38-48%), K-feldspar (2-5%), biotite (16-20%) and the monzogranite is composed of quartz (30-34%), plagioclase (~26%), K-feldspar (35-39%), biotite (3-4%). Zircon, apatite, and opaques occur as accessory minerals, while sericite, muscovite, chlorite, and epidote occur as secondary minerals. Plagioclase occurs as phenocrysts larger than 5 mm, exhibit a polysynthetic twin, and are usually replaced by sericite and saussurite (Figure 6c). They present microfractures (Figure 6c) and deformed twins, in addition to restricted kink-bands; subhedral crystals (0.8-2.5 mm) also occur, which are usually replaced by sericite and are associated with smaller crystals of quartz and K-feldspar.

K-feldspar occurs as phenocrysts >5 mm, with perthitic exsolution and/or chessboard twin; medium subhedral crystals (0.8-2.0 mm) with chessboard twins locally deformed. Also, they exhibit perthitic exsolution of diverse morphologies.

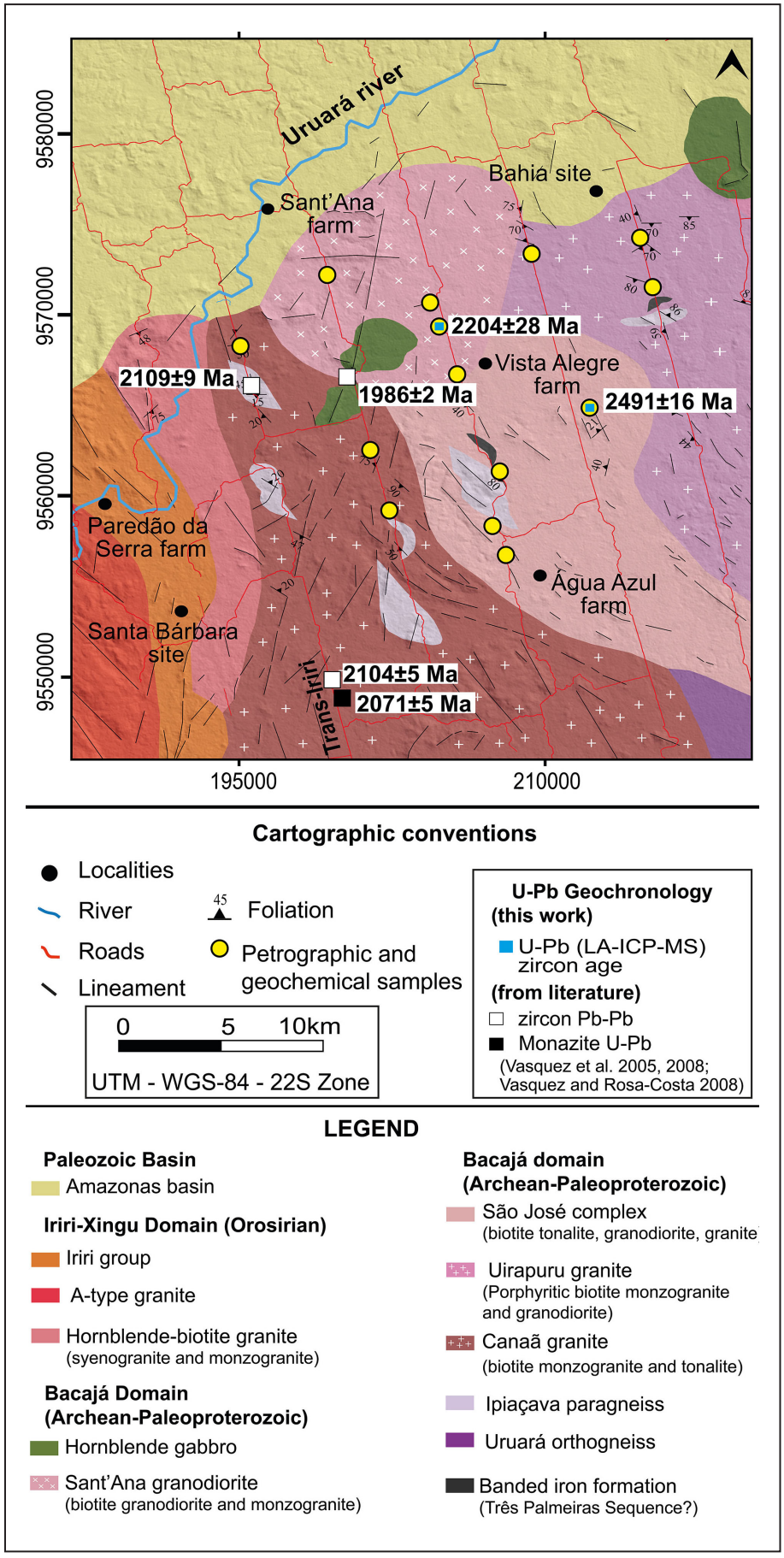

FIGURE 2 – Geological map of the study area made with data acquired in the fieldwork, geophysical, and remote sensing data.

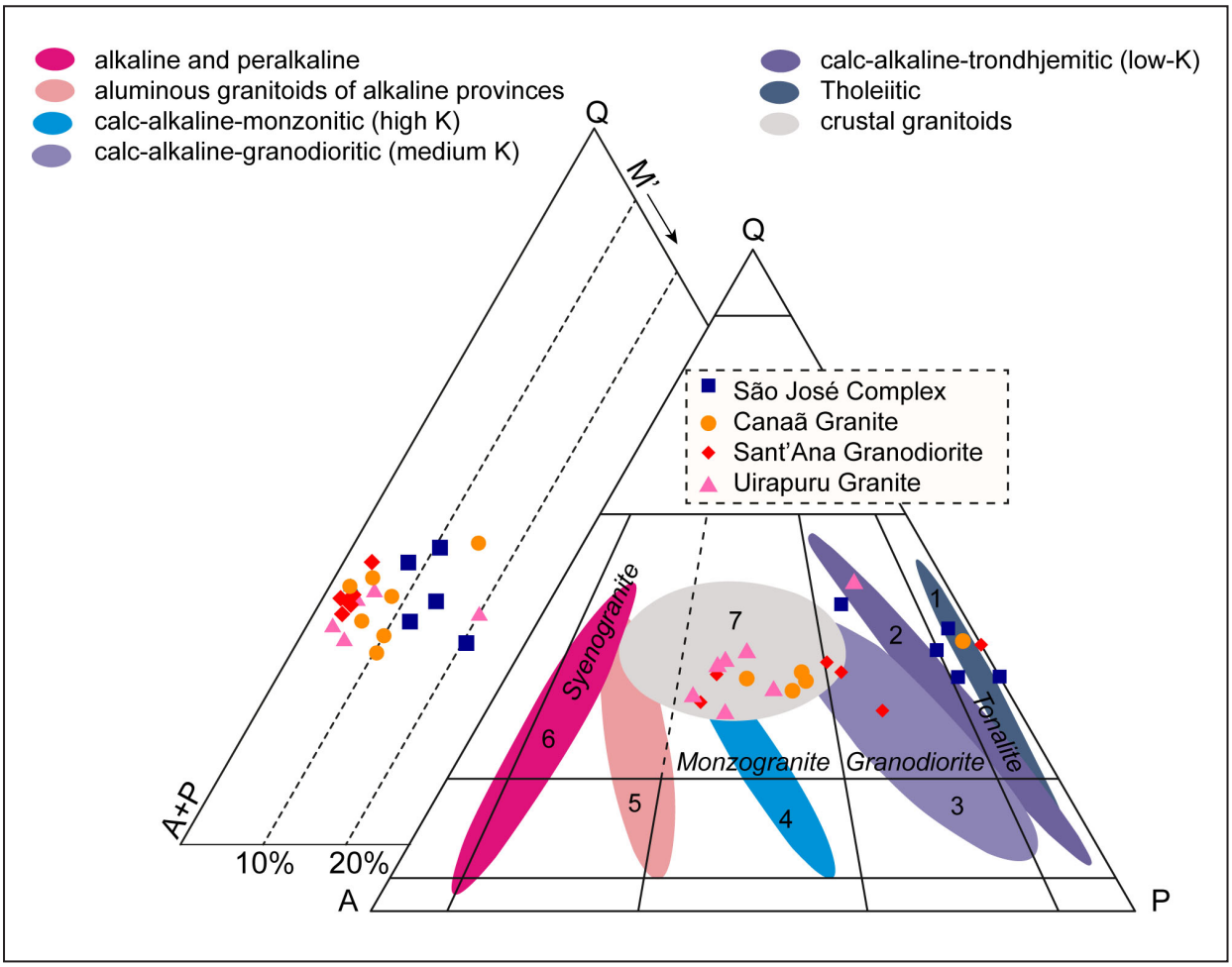

FIGURE 3 – QAP and Q-(A+P)-M' diagrams (Streckeisen 1976) with the modal composition of the studied granitoids and compositional trends of the Lameyre and Bowden (1982) magmatic series: (1) Toleiitic series, (2) low-K Calc-Alkaline series, (3) Medium and high-K calc-alkaline series, (4) Shoshonitic series, (5) Metaluminous supersaturated alkaline series, (6) Supersaturated alkaline series, (7) Peraluminous leucocratic association. M' = Mafic Minerals (Biotite + Opaque).

Quartz occurs as prismatic subhedral crystals (2.5 - 4.0 mm) with undulose extinction (Figure 6e); and, as tiny crystals (0.2-2.0 mm), recrystallized in subgrains (Figure 6d), usually associated with biotite, muscovite, and epidote and at the edges of larger feldspar and quartz crystals. Biotite forms subhedral lamellar crystals (0.8-2.0 mm) partially replaced by chlorite that forms mafic clusters associated with epidote, allanite, chlorite, opaques, and muscovite that are irregularly distributed among the larger feldspar and quartz crystals (Figure 6d). Another way that biotite occurs is as fine recrystallized crystals related to quartz crystals (Figure 6e). Zircon occurs as small prismatic crystals included in K-feldspar, plagioclase, and biotite. Apatite occurs as inclusions mainly in plagioclase. Opaque minerals (Figure 6f) form subhedral crystals associated with biotite and are usually replaced by epidote.

4.1.4. Uirapuru Granite

It consists predominantly of biotite monzogranites with muscovite, subordinate syenogranites, and granodiorites, exhibiting dark gray color, inequigranular coarse to porphyritic (Figure 7a-b). They usually present foliation marked by biotite, quartz, and feldspar porphyroclasts. This unit is cross-cut by aplitic dykes veins of quartz and epidote. Monzogranite consists of quartz (25-33%), plagioclase (21-30%), K-feldspar (25-34%), and biotite (4-11%). Zircon, apatite, epidote, opaque and muscovite occur as accessory minerals, while sericite, muscovite, chlorite, and epidote occur as secondary minerals.

Plagioclase forms euhedral to subhedral phenocrysts with dimensions above 5 mm (Figure 7c), usually presenting a polysynthetic twin. It is common to be heavily sericitized in some regions (Figure 7c-d). Quartz occurs as a medium to coarse subhedral to anhedral crystals (Figure 7d), in addition to elongated crystals that eventually form a ribbon quartz texture. There are also crystals recrystallized in subgrains that mark a mylonitic texture (Fig. 7d). Biotite and muscovite form medium to coarse euhedral to subhedral crystals (Figure 7c-d), usually tabular that exhibit straight to serrated contact with K-feldspar and plagioclase. Another way they occur is usually as small, dispersed crystals associated with recrystallized quartz marking the foliation. Biotite is locally replaced by chlorite. K-feldspar, as well as plagioclase, also occurs as euhedral to subhedral phenocrysts (>5 mm), exhibits perthitic texture, and chessboard twins that are usually deformed (Figure 7f). Eventually, the phenocrysts exhibit microfractures where they tend to form new grains. At the edges, the phenocrysts reveal core-like texture, and locally they show plagioclase inclusions (Figure 7e).

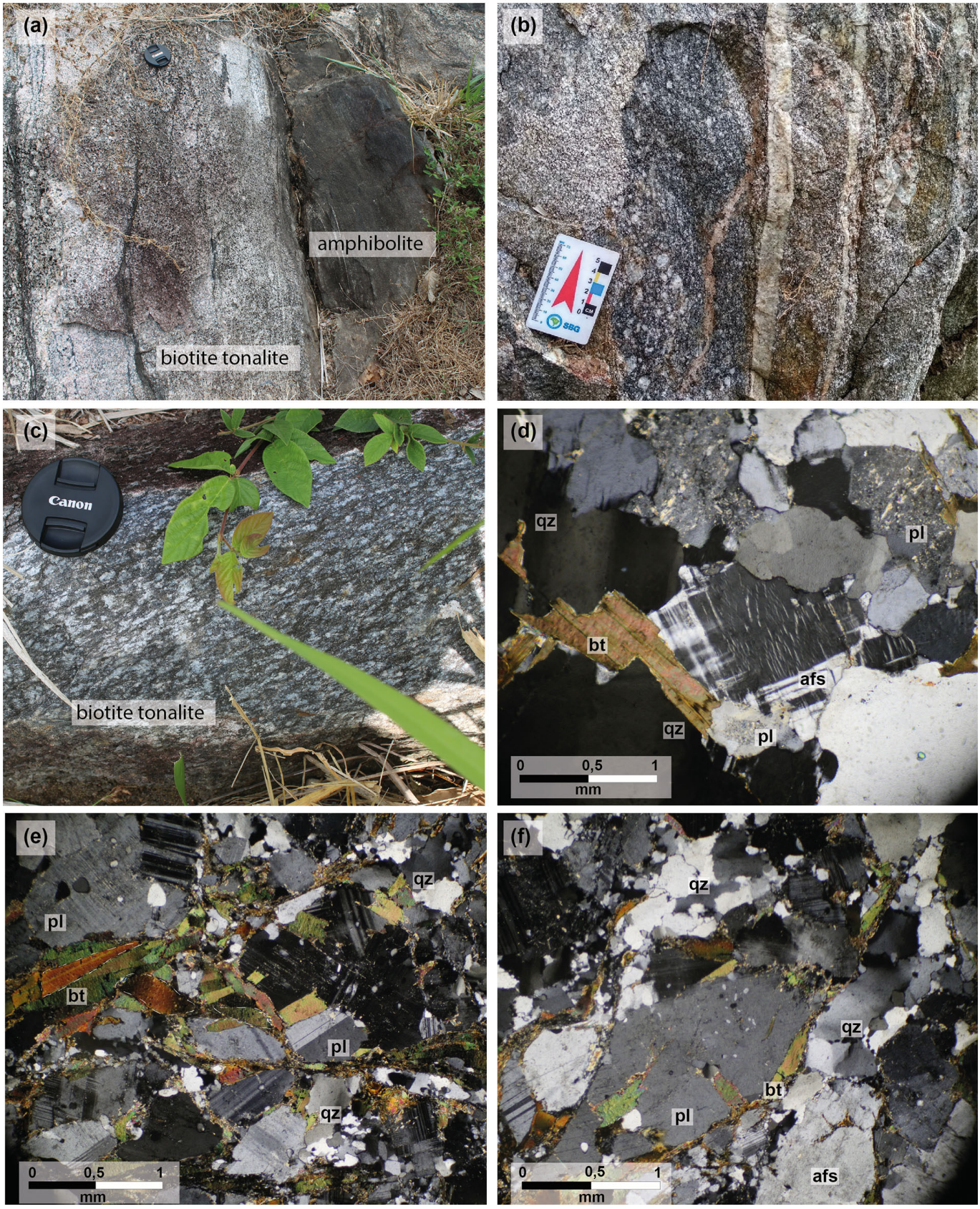

FIGURE 4 – Mesoscopic and petrographic features of the São José Complex (a) biotite tonalite block with amphibolite metric xenolith; (b) biotite tonalite cut by finer-grained granitic aplitic dikes; (c) biotite tonalite with oriented plagioclase crystals marking the submagmatic foliation; (d) photomicrograph showing the textural weave of the biotite tonalite; (e) photomicrograph of a section with foliated biotite tonalite showing biotite-fish and quartz subgrains; (f) petrographic section with the presence of plagioclase porphyroclasts with inclusions of biotite and quartz.

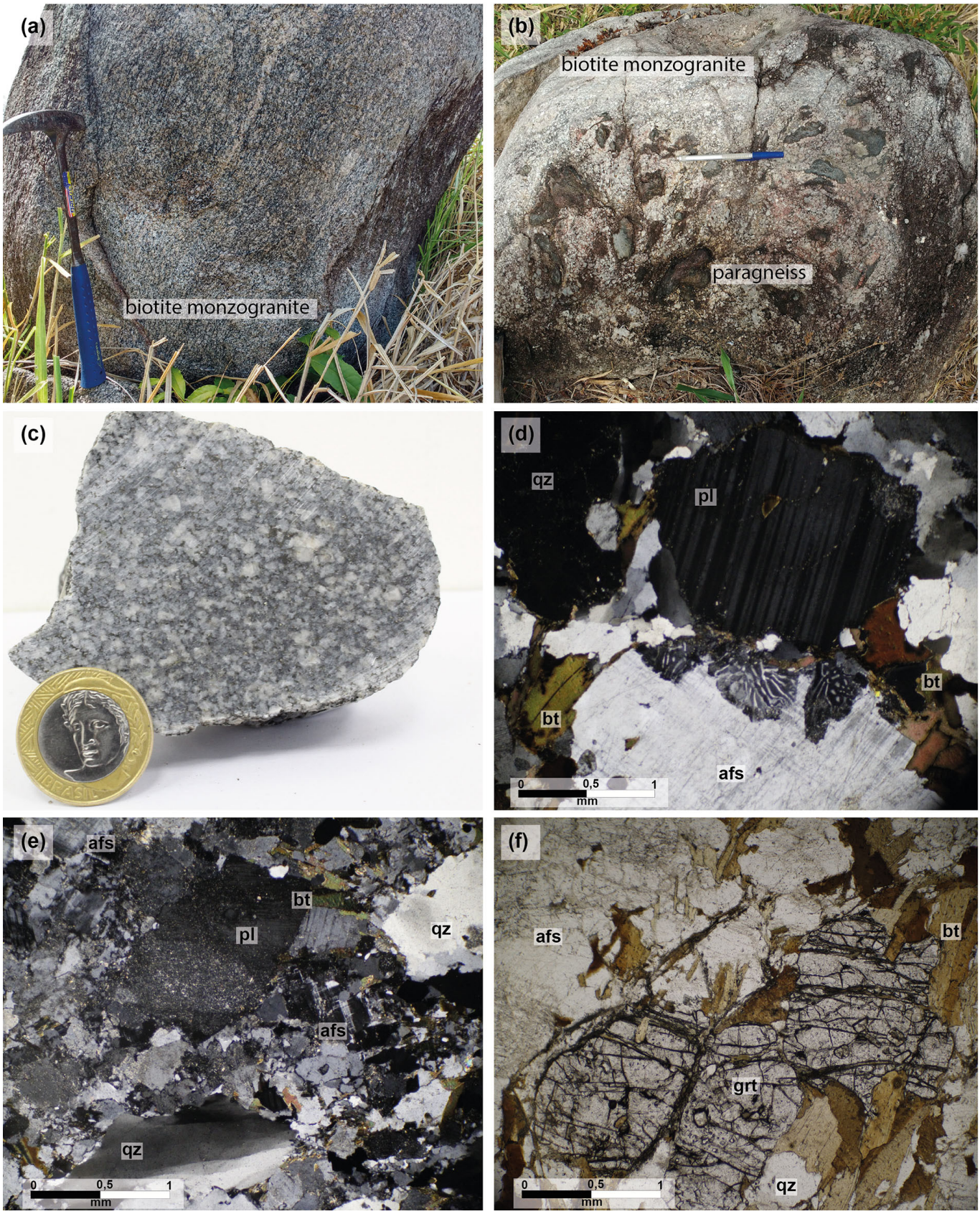

FIGURE 5 – Field features and petrographic aspects of Canaã Granite; (a) biotite monzogranite block with submagmatic foliation marked by biotite alignment; (b) outcrop view with the presence of centimetric angular xenoliths of kyanite-biotite gneiss; (c) medium grained biotite monzogranite sample with plagioclase and K-feldspar phenocrysts; (d) photomicrograph showing the inequigranular textural weave of the biotite monzogranite with the presence in the center of the image of myrmekite texture; (e) photomicrograph showing biotite monzogranite with plagioclase crystals replaced by sericite, quartz with undulose extinction and subgrains; (f) photomicrograph with fractured garnet crystals associated with biotite crystals.

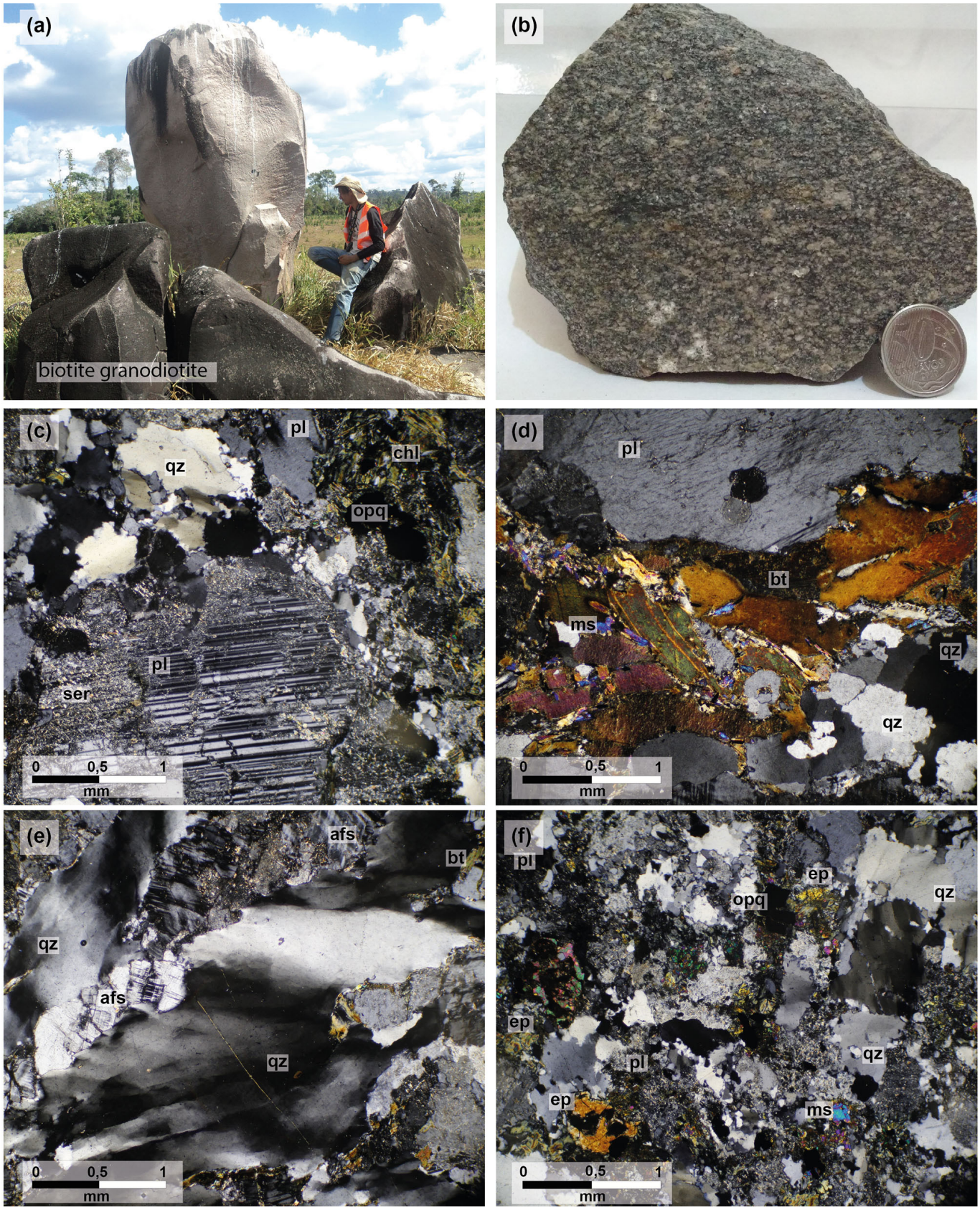

FIGURE 6 – Field features and petrographic aspects of Sant'Ana Granodiorite; (a) outcrop of Granodiorite Sant'Ana; (b) sample of biotite granodiorite collected; (c) biotite granodiorite photomicrograph with emphasis on the plagiclase phenocryst that exhibits microfractures and its edges are replaced by sericite, in addition to anhedral quartz crystals with subgrain migration in the upper region; (d) photomicrograph of granodiorite showing a section with clusters of biotite, quartz and muscovite; (e) photomicrograph with quartz crystal with undulose extinction at its edges quartz presents small grains of K-feldspar, quartz and biotite; (f) finer-grained micrographic section showing opaque mineral crystals, muscovite and epidote.

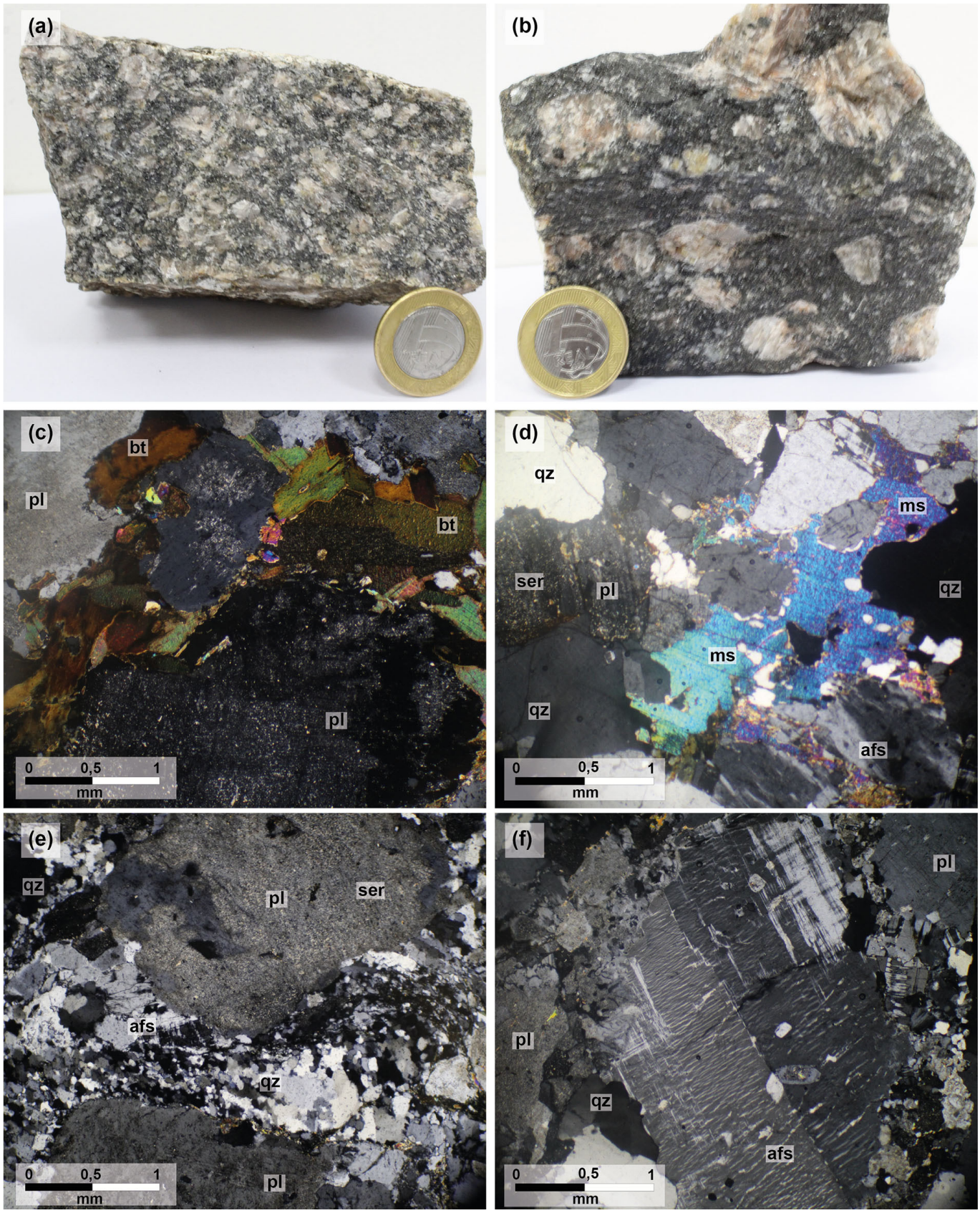

FIGURE 7 – Field samples and petrographic aspects of the Uirapuru Granite; (a-b) samples of coarse-grained biotite monzogranite and porphyritic biotite syenogranite; (c) textural web of an inequigranular biotite monzogranite with plagioclase crystals substituted for sericite and lamellar subhedral biotite; (d) textural web of a biotite monzogranite exhibiting large lamellar muscovite crystals and fine quartz between the plagioclase crystals; (e) textural plot with plagioclase phenocrysts with small quartz and K-feldspar grains that form mylonitic texture; (f) euhedral phenocryst of pertitic K-feldspar with small plagioclase inclusions, the crystal is also bordered by small quartz grains.

4.2. Whole-rock geochemistry

The analyses of the major, trace, including rare earth elements, of the granitoids from this study are presented in Table 2 and plotted in Harker's diagrams in Figures 8 and 9.

4.2.1. São José Complex

Four samples of the São José Complex (CVM-28, CVM-33, CVM-36, CVM-29) were examined in this study. They have variable SiO_2 content (66.55-71.23%) and plot in the fields of tonalites, granodiorites, and granites (Figure 10a) in the P-Q diagram of Debon and Le Fort (1983). They are slightly peraluminous (A/CNK=1.08-1.09; Figure 10b). Two samples fall in the high-K calc-alkaline field, one in the medium-K calc-alkaline and another is part of the shoshonitic series in the K_2O diagram versus SiO_2 (Figure 10c).

In the diagram of major elements (Al_2O_3 + CaO) / (FeOt + Na_2O + K_2O) versus 100 (MgO + FeOt + TiO_2) / SiO_2 (Sylvester 1989) two samples plot in the field of high fractionated calc-alkaline granite (Figure 10d). They are characterized by K_2O content ranging from 1.47 to 5.53 wt%. The samples display a K_2O/Na_2O ratio between 0.36 and 1.52 (Table 2).

The content of Al_2O_3 and Na_2O range from 14.96-17.73 wt % and 3.37-4.54 wt %, respectively, whereas CaO varies from 1.0-4.57 wt % (Table 2). The samples exhibit negative correlations between SiO_2 content versus Al_2O_3, FeOt, CaO and P_2O_5, and positive correlations with K_2O (Figure 8). In the FeOt/(FeOt+MgO) versus SiO_2 (Frost et al. 2001) diagram the samples plot in the magnesium field (Figure 10e), with the values of Mg# between 33.67 and 40.05 and FeOt / (FeOt + MgO) ratios between 0.73 and 0 .78.

In the mantle normalized trace element diagram (McDonough and Sun 1995), the samples from the São José Complex are enriched in lithophile elements of large ionic radius (Ba and Rb), U, and Pb and depleted in Nb, Ta, P and Ti (Figure 11a). They exhibit high Sr content (329-662 ppm) except for one sample (Sr = 127 ppm), moderate Rb (130-279 ppm), low K/Rb ratios (113.08-245.78 ppm), Rb/Sr (0.20-0.55), Rb/Ba (0.15-0.25) and moderate Sr/Y (13.26-39) (Table 2).

The sum of rare earth elements ranges from 161 to 385 ppm. In the mantle normalized rare earth elements diagrams

TABLE 2 – Whole-rock geochemical analysis of major, trace, and rare earth elements of the studied granitoids

	São José Complex				Uirapuru Granite			Sant'Ana Granodiorite				Canaã Granite		
	Bt-Tnt	Bt-Tnt	Bt-Grd	Bt-Tnt	Bt-Mzg	Bt-Mzg	Bt-Mzg	Bt-Grd	Bt-Mzg	Bt-Grd	Bt-Mzg	Bt-Mzg	Bt-Mzg	**Bt-Tnt**
	CVM-28	CVM-33	CVM-26	CVM-29	CVM-38	CVM-31	CVM-36	CVM-04	CVM-21	CVM-24	CVM-18	CVM-14	CVM-15	CVM-07
Major elements (wt%)														
SiO_2	66.53	68.56	71.78	71.23	68.89	70.66	71.43	70.53	70.67	71.35	72.72	73.63	73.83	73.92
TiO_2	0.42	0.40	0.17	0.20	0.65	0.55	0.40	0.56	0.35	0.20	0.23	0.19	0.18	0.24
Al_2O_3	17.73	15.26	14.96	15.89	13.74	13.32	13.77	14.33	14.67	14.87	14.19	14.17	13.9	13.64
Fe_2O_3t	3.19	3.87	1.46	1.58	4.49	3.88	3.11	2.69	2.42	1.62	1.91	1.52	1.43	1.59
MnO	0.037	0.05	0.011	0.009	0.047	0.045	0.026	0.019	0.019	0.016	0.021	0.021	0.014	0.013
MgO	1.16	1.45	0.42	0.45	0.6	0.61	0.44	0.7	0.42	0.3	0.28	0.47	0.25	0.31
CaO	4.57	2.64	1	2.13	2.05	1.67	1.16	1.74	0.89	0.97	1.09	1.64	0.99	1.02
Na_2O	4.07	3.37	3.65	4.54	2.7	2.52	2.73	3.21	2.98	3.55	3.45	3.9	3.36	3.16
K_2O	1.47	3.49	5.53	3.27	5.68	5.49	5.61	5.16	6.52	6.15	5.16	3.58	5.32	5.2
P_2O_5	0.12	0.13	0.08	0.06	0.22	0.17	0.15	0.18	0.08	0.08	0.06	0.05	0.06	0.06
LOI	0,45	0,47	0,64	0,32	0,60	0,76	0,91	0,57	0,70	0,65	0,62	0,56	0,39	0,55
A/CNK	1.08	1.09	1.09	1.07	0.98	1.03	1.10	1.04	1.09	1.05	1.08	1.07	1.07	1.08
K_2O/Na_2O	0.36	1.04	1.52	0.72	2.10	2.18	2.05	1.61	2.19	1.73	1.50	0.92	1.58	1.65
K_2O + Na_2O	5.54	6.86	9.18	7.81	8.38	8.01	8.34	8.37	9.5	9.7	8.61	7.48	8.68	8.36
Mg#	39.33	40.05	33.90	33.67	19.24	21.89	20.14	31.69	23.63	24.82	20.72	35.53	23.76	25.79
FeOt / (MgO + FeOt)	0.73	0.73	0.78	0.78	0.88	0.86	0.88	0.79	0.85	0.84	0.87	0.76	0.85	0.84
Trace elements (ppm)														
Li		87.3		38.3	32.4	14.9			21.0	15.5		13.7	14.2	
Be		1.55		2.02	2.79	2.29			1.13	0.97		2.00	1.21	
Sc		10.9		4.55	8.15	4.48			2.30	1.39		2.75	1.09	
V	52	56.1	23.7	16.2	33.6	26.7	27.2	35	7.9	8.2	11.5	14.8	9.2	16.6
Cr	18.7	56.3	35	16.5	11.7	13.5	13.3	46	6.94	14.5	66	17.4	9.77	20.1
Co		8.68		4.07	4.40	3.39			1.30	1.07		1.93	0.86	
Ni	4.7	12.8	3.7	1.94	2.46	2.31	5	5.6	0.45	2.38	2.7	2.61	1.32	2.7
Cu	6.5	15.8		1.44	5.64	4.54		4	0.38	0.48		0.93	1.10	7.8
Zn	67	72.7	50	60.8	61.5	44.0	80	85	137	138	68	136	15.9	37
Ga	24.5	19.1	21.9	23.4	23.3	21.0	21.4	24	22.1	19.0	24.2	16.3	16.9	20.2

TABLE 2 – Whole-rock geochemical analysis of major, trace, and rare earth elements of the studied granitoids (contined)

	São José Complex				Uirapuru Granite			Sant'Ana Granodiorite				Canaã Granite		
	Bt-Tnt	Bt-Tnt	Bt-Grd	Bt-Tnt	Bt-Mzg	Bt-Mzg	Bt-Mzg	Bt-Grd	Bt-Mzg	Bt-Grd	Bt-Mzg	Bt-Mzg	Bt-Mzg	**Bt-Tnt**
	CVM-28	CVM-33	CVM-26	CVM-29	CVM-38	CVM-31	CVM-36	CVM-04	CVM-21	CVM-24	CVM-18	CVM-14	CVM-15	CVM-07
Rb	130	160	225	279	232	147	260	206	230	206	248	102	144	211
Sr	662	329	127	511	151	126	134	298	85.1	63.5	101	266	83.8	121
Y	4.2	24.8	7.6	13.1	44.0	29.8	21.9	5.9	8.99	5.25	3.5	13.3	8.12	13.1
Zr	97	222	170	90.4	485	347	244	283	280	82.3	140	123	131	150
Nb	6.8	9.40	10.6	7.36	19.8	16.5	19.6	8.1	9.00	10.8	8.9	6.74	8.04	9.9
Mo		1.11		0.60	4.13	1.83			0.45	1.89		0.36	0.57	
Cd		0.26		0.10	0.29	0.25			0.17	0.03		0.10	0.09	
Sn		1.75		1.33	3.10	1.68			1.36	1.39		0.92	0.53	
Sb		0.02		0.01	0.01	0.02			0.02	0.02		0.01	0.01	
Cs		6.61		2.17	2.13	1.02			2.14	1.10		1.20	1.02	
Ba	520	1060	607	1055	1236	1012	927	1103	709	335	596	589	763	910
Hf		5.04		2.18	10.58	8.04			7.23	2.45		3.24	3.54	
Ta		0.82		0.61	0.93	0.68			0.63	0.63		0.74	0.33	
W		2.96		1.19	2.28	1.51			0.86	0.65		0.90	0.41	
Pb	5.9	25.3	46	43.0	25.1	22.2	46	52	49.0	32.9	56	21.2	21.9	40
Bi		0.25		0.12	0.08	0.05			0.27	0.06		0.03	0.03	
Th		9.84		20.6	28.3	36.3			98.7	31.3		3.40	20.1	
U		3.44		3.09	2.17	1.81			11.4	14.9		6.74	2.38	
K/Rb	113.08	218.02	245.78	117.18	245.31	373.53	215.77	250.49	283.94	299.16	208.06	350.43	370.61	246.45
Rb/Sr	0.20	0.49	1.77	0.55	1.53	1.17	1.94	0.69	2.70	3.24	2.46	0.38	1.71	1.74
Rb/Ba	0.25	0.15	0.37	0.26	0.19	0.15	0.28	0.19	0.32	0.61	0.42	0.17	0.19	0.23
Sr/Y	157.62	13.26	16.71	39.00	3.44	4.22	6.12	50.51	9.46	12.10	28.86	19.99	10.33	9.24
Nb/Ta		11.46		12.05	21.31	24.37			14.38	17.23		9.09	24.51	
Rare Earth Elements (ppm)														
La		35.8		93.7	117	156			126	34.1		11.4	38.9	
Ce		70.6		197	202	270			223	69.0		18.9	65.6	
Pr		7.23		16.5	25.6	30.0			20.8	8.28		1.95	6.67	
Nd		26.2		55.4	91.6	96.9			65.2	29.5		6.7	21.6	
Sm		4.80		8.57	15.6	12.8			9.90	5.86		1.25	3.47	
Eu		1.05		1.46	1.66	1.35			0.51	0.32		0.63	0.39	
Gd		4.52		6.47	13.25	10.34			6.81	4.20		1.30	3.00	
Tb		0.64		0.67	1.67	1.14			0.56	0.40		0.23	0.36	
Dy		4.00		3.00	8.74	5.69			2.11	1.42		1.73	1.69	
Ho		0.86		0.45	1.62	1.06			0.32	0.20		0.42	0.28	
Er		2.59		1.00	4.24	2.90			0.83	0.41		1.51	0.70	
Tm		0.39		0.11	0.55	0.38			0.11	0.05		0.29	0.08	
Yb		2.69		0.56	3.26	2.34			0.70	0.26		2.37	0.51	
Lu		0.41		0.08	0.46	0.35			0.09	0.04		0.38	0.07	
ΣETR		161.00		385.02	487.13	591.14			456.41	153.97		49.05	143.28	
ΣLREE		144.65		371.23	451.68	565.60			444.38	146.68		40.20	136.20	
ΣHREE		17.16		13.79	35.44	25.55			12.04	7.30		8.85	7.07	
LREE/HREE		8.43		26.92	12.74	22.14			36.92	20.10		4.54	19.26	
Eu/Eu*		0.64		0.55	0.33	0.33			0.17	0.17		1.41	0.34	
$(La/Sm)_N$		4.66		6.83	4.70	7.61			7.96	3.63		5.71	7.01	
$(Gd/Yb)_N$		1.34		9.27	3.25	3.53			7.81	12.88		0.44	4.75	
$(La/Yb)_N$		8.88		111.92	23.95	44.30			120.34	87.01		3.21	51.33	

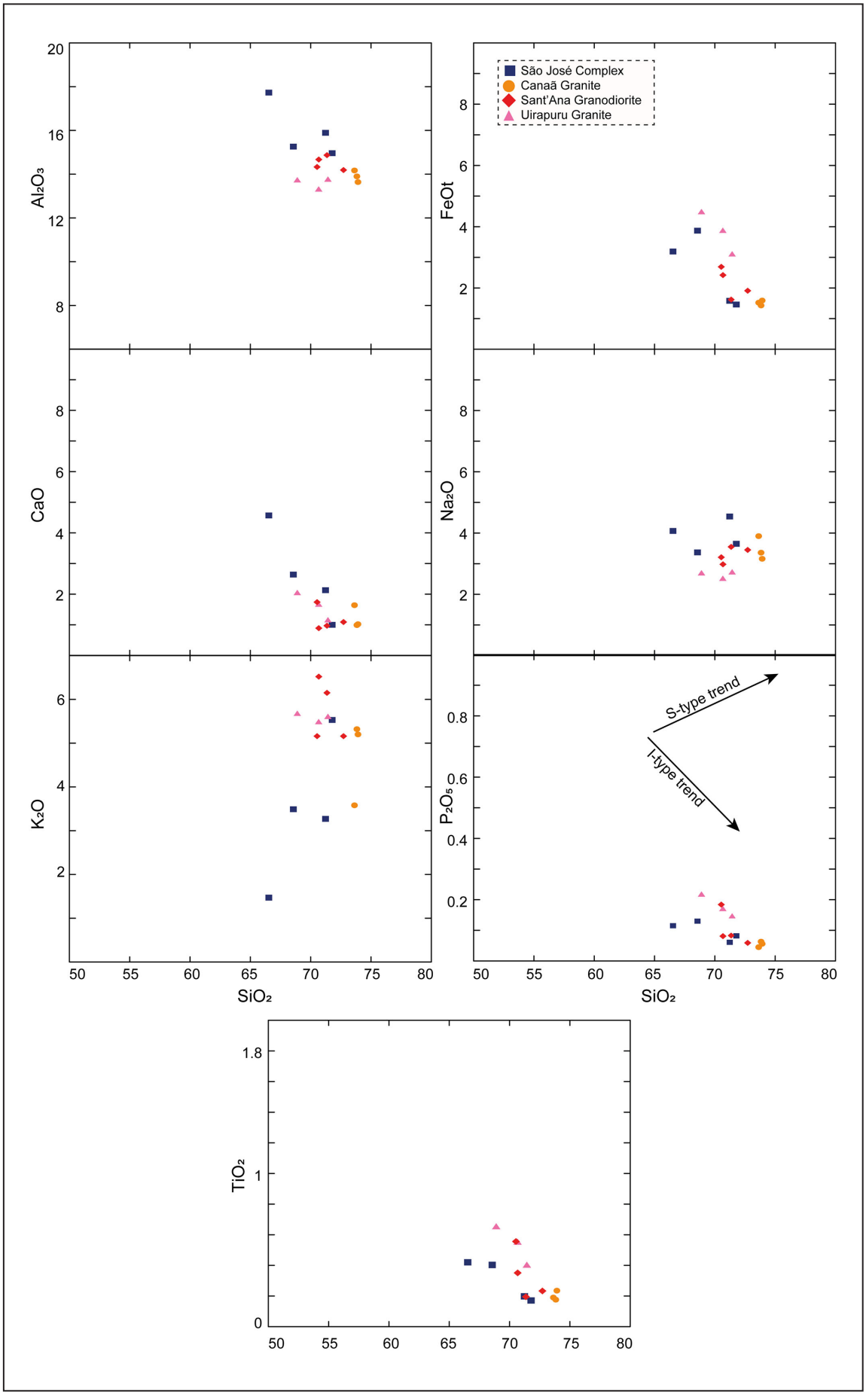

FIGURE 8 – Harker's diagram of major elements for the analyzed granitoids of the northwestern Bacajá Domain.

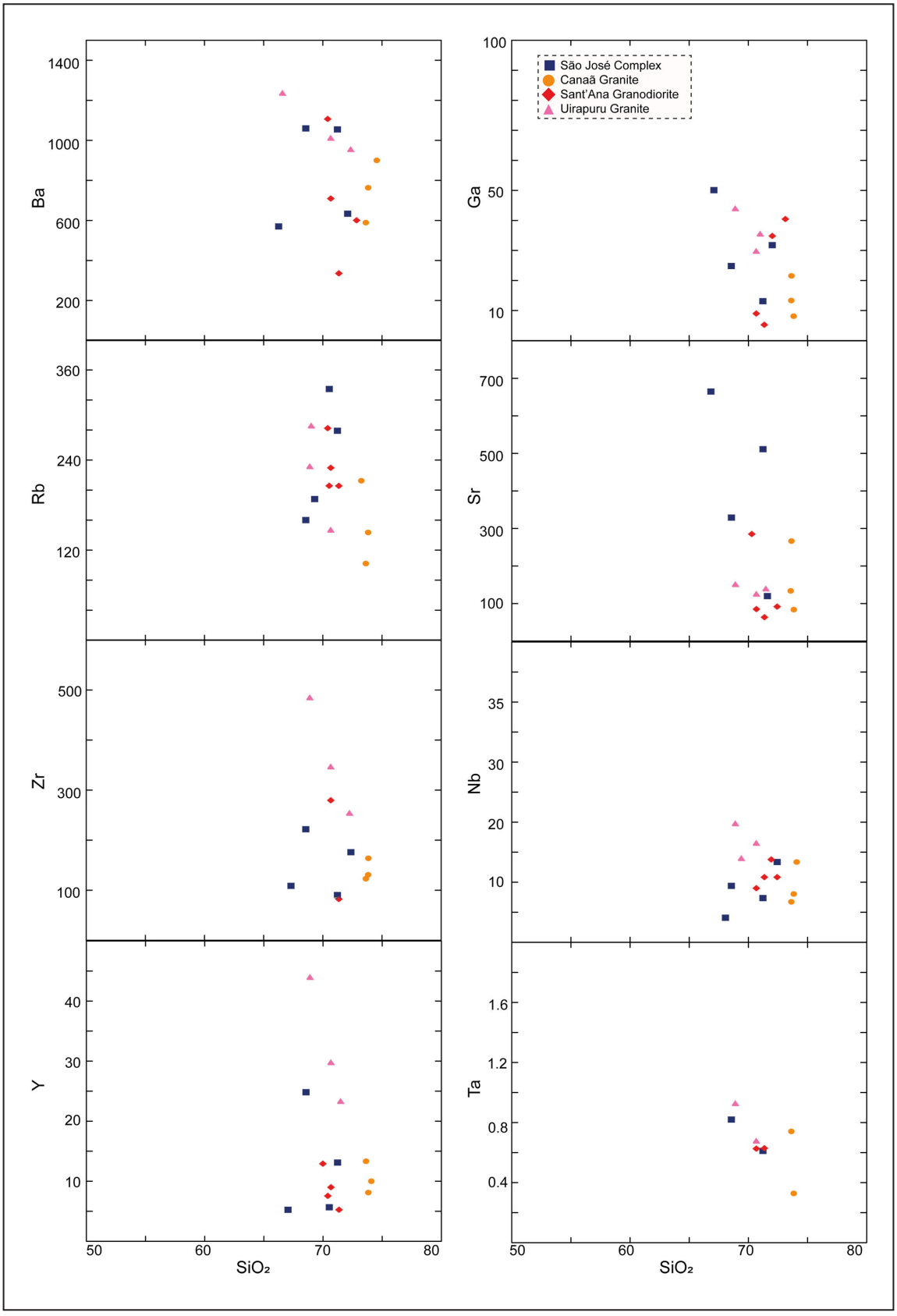

FIGURE 9 – Harker's diagram of trace elements for the analyzed granitoids of the northwestern Bacajá Domain.

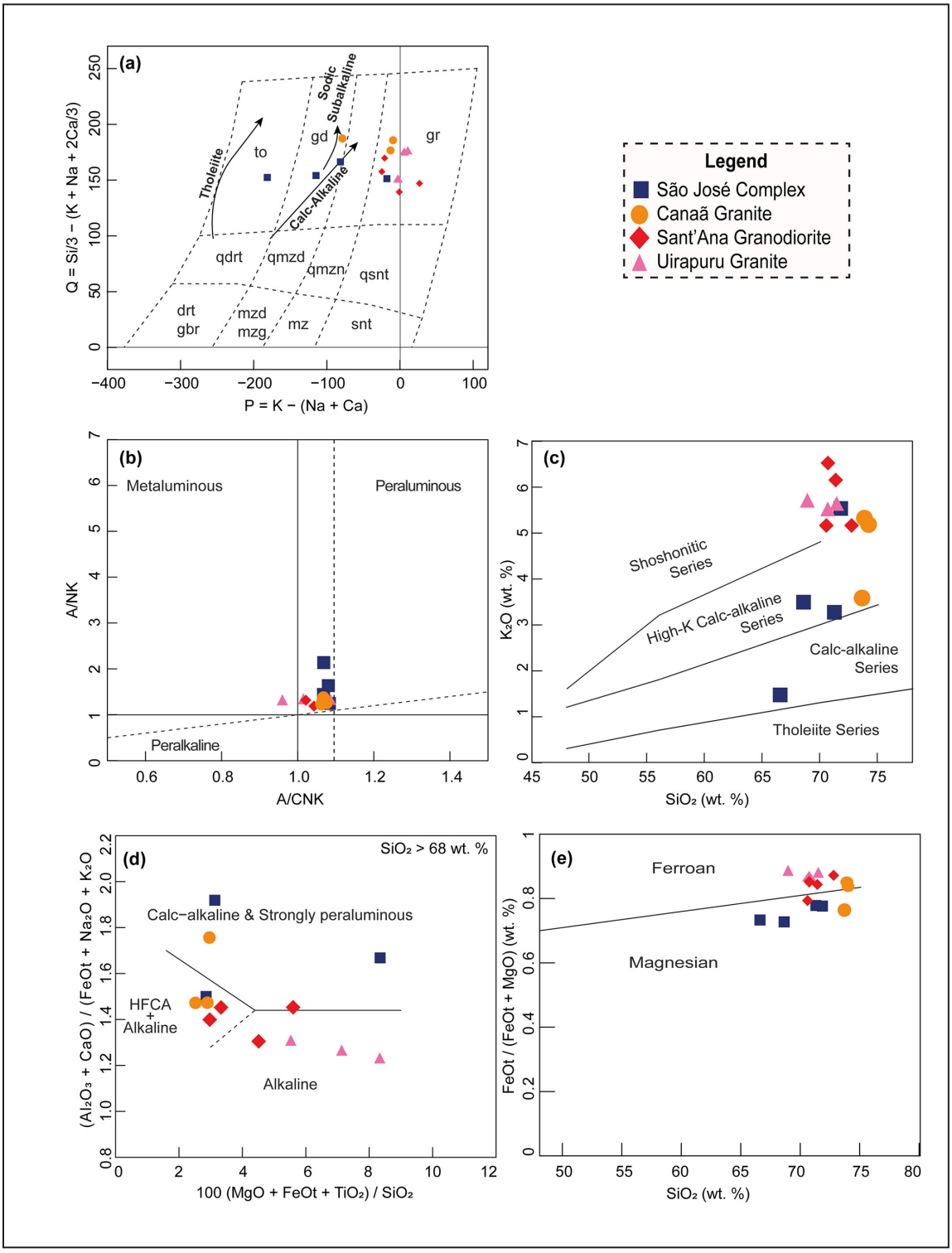

FIGURE 10 – Geochemical classification diagrams for the granitoids of the northwestern Bacajá. (a) P-Q diagram (Debon and Le Fort 1983); (b) A/NK versus A/CNK diagram by Maniar and Piccolli (1989); (c) K_2O versus SiO_2 diagram by Peccerillo and Taylor (1976) for classification of magmatic series; (d) discriminant diagram of major elements (Al_2O_3 + CaO) / (FeOt + Na_2O + K_2O) versus 100 (MgO + FeOt + TiO_2) / SiO_2 of Sylvester (1989) for classification of granites into calc-alkaline and alkaline series for the study rocks; (e) FeOt/(FeOt+MgO) versus SiO_2 diagram of Frost et al. (2001) for the classification of granitoids into ferrous or magnesian.

(McDonough and Sun 1995) the samples exhibit weak negative Eu anomalies (Eu*/Eu = 0.55-0.64). These samples are enriched in light rare earth elements ((La/Yb)N = 8.88-111.92), with moderate fractionation of light to heavy rare earth elements ((La/Sm)N = 4.66-6.83; (Gd/Yb)N = 1.34-9.27) (Figure 11a).

In the granite typology classification diagrams (Whalen et al. 1987), the samples predominantly plot in the field of I-S-type granites (Figure 12a-d). In the diagram $FeO_t/(FeO_t+MgO)$ versus Al_2O_3 of Dall'Agnol and Oliveira (2007), which divides the granites between calc-alkaline granites and reduced and oxidized A-type granites (Figure 12e), the rocks of the São José Complex are classified in the field of calc-alkaline granites. The samples plot mainly in the volcanic arc and/or syn-collisional environments (Figures 13a-d; Pearce et al. 1984; Pearce 1996).

4.2.2. Canaã Granite

Three samples of the Canaã Granite (CVM-07, CVM-14, CVM-15) were analyzed. They have a high and restricted variation of SiO_2 content (73.63-73.92 wt%). These samples plot in the granodiorite and granite fields (Figure 10a) in the P-Q diagram of Debon and Le Fort (1983) and are slightly peraluminous (A/CNK=1.07-1.08; Figure 10b). In the K_2O versus SiO_2 diagram, one sample has affinity for the high-K calc-alkaline series, while the other two plot at the boundary of the high-K and shoshonitic calc-alkaline series fields (Figure 10c). In the diagram $(Al_2O_3 + CaO) / (FeOt + Na_2O + K_2O)$ versus $100 (MgO + FeOt + TiO_2) / SiO_2$ (Sylvester 1989), two samples exhibit affinity with the fractionated calc-alkaline to calcium-alkaline series, while the other plots in the field from calc-alkaline to strongly peraluminous rocks (Figure 10d).

The Canaã Granite is characterized by a K_2O ranging from 3.58 to 5.32 wt%, K_2O/Na_2O ratio between 0.92 and 1.65 wt%, Al_2O_3 (13.64-14.17 wt%), Na_2O (3.16-3.90 wt%), and CaO (0.99-1.64 wt%). Samples show weak negative correlations between SiO_2 content versus Al_2O_3, CaO and Na_2O and a positive correlation with P_2O_5 (Figure 8). The values of MgO vary between 0.25-0.47 wt%. In the FeOt/(FeOt+MgO) versus SiO_2 (Frost et al. 2001) diagram, two samples plot in the field of magnesian granites and one in the ferrous granites (Figure 10e), Mg# values range from 25.76 to 35.53 and FeO_t / (MgO + FeO_t) from 0.76 to 0.84.

In the mantle normalized trace element diagram (McDonough and Sun 1995), the Canaã Granite samples are enriched in lithophile elements of large ionic radius (Ba and Rb), U, Pb and depleted in Nb, Ta, P and Ti (Figure 11b). They show low to moderate Sr content (82.8-266 ppm), Rb (102-211 ppm), with moderate to high K/Rb ratios (246.45-370.61 ppm), high Rb/Sr ratio (1.71-1.74) except for a sample with low Rb/Sr ratio (0.38), low Rb/Ba ratio (0.17-0.23), moderate Sr/Y (9.24-19.99) (Table 2).

The total sum of rare earth elements is low and varies between 49.05 and 143.28 ppm. In the mantle normalized rare earth element diagram (McDonough and Sun 1995) the two analyzed samples exhibit distinct Eu anomalies, one with a strong negative anomaly (Eu*/Eu = 0.34), and other with positive anomaly (Eu*/Eu = 1.41) (Figure 11b'). The La/Yb ratios range from 3.21 to 51.33), with moderate to high fractionation of light to heavy rare earth elements ($(La/Sm)_N$ = 5.71-7.01; $(Gd/Yb)_N$ = 0.44-4.75).

The Canaã Granite rocks are classified as I-S type granites (Figure 12a-d; Whalen et al. 1987). In the diagram $FeO_t/(FeO_t+MgO)$ versus Al_2O_3 (Dall'Agnol and Oliveira 2007), two of them plot in the field of calc-alkaline granites and one in the field of oxidized A-type granites (Figure 12e). According to the discriminant diagrams of tectonic environments, the samples are classified mainly in the volcanic arc and/or syn-collisional granite environments (Figure 13a-d; Pearce et al. 1984; Pearce 1996).

4.2.3. Sant'Ana Granodiorite

Four samples of Sant'Ana Granodiorite lithostratigraphic unit (CVM-04, CVM-21, CVM-24, CVM-18) were analyzed. They have high SiO_2 content (70.53-72.72 wt%) and plot in the granite fields (Figure 10a; Debon and Le Fort 1983). They are slightly peraluminous (A/CNK= 1.04-1.09; Figure 10b). In the K_2O versus SiO_2 diagram (Peccerillo and Taylor 1976), the samples have an affinity with the shoshonitic series (Figure 10c), while in the $(Al_2O_3 + CaO) / (FeO_t + Na_2O + K_2O)$ versus $100 (MgO + FeOt + TiO_2) / SiO_2$ diagram (Sylvester 1989) two samples fall in the field of the fractionated calcium-alkaline series and another two in the field of the alkaline series (Figure 10d).

The analyzed samples are characterized by K_2O content between 5.16 and 6.52 wt% with K_2O/Na_2O ratio ranging from 1.50 to 2.19. Contents of Al_2O_3, Na_2O and CaO ranging between 14.19-14.87 wt%, 2.98-3.55 wt% and 0.89-1.74 wt%, respectively. Negative correlations between SiO_2 content versus FeO_t, K_2O, and P_2O_5 (Figure 8) is also observed. In the $FeO_t/(FeO_t+MgO)$ versus SiO_2 diagram (Frost et al. 2001), three samples plot in the field of ferrous granites and one in the field of magnesian granites (Figure, 10e), the values of Mg# vary between 20.72 and 31.69 and those of $FeO_t/(FeO_t+MgO)$ between 0.79 and 0.87.

In the mantle normalized multielement diagram (McDonough and Sun 1995), the Sant'Ana Granodiorite is enriched in Rb, Th, U, La, Pb, Nd, Zr, Dy; depleted in Ba, Nb, Ta, Sr and P and Ti (Figure 11c). They exhibit low to moderate Sr content (63.50-298 ppm), moderate to high Rb content (206-248 ppm), with high K/Rb ratios (208.06-299.16 ppm), high Rb ratio /Sr (2.46-3.24 ppm), except for a sample with a low Rb/Sr ratio (Rb/Sr = 0.68), high Rb/Ba ratio (0.32-0.61), with the exception of one sample (Rb/Ba = 0.19), moderate to high Sr/Y ratio (9.46-50.51) (Table 2).

The sum of rare earth elements is high and ranges from 153.97 to 456.41 ppm. In the mantle normalized diagram for rare earth elements (McDonough and Sun 1995), the samples are enriched in light relative to heavy rare earth elements ($(La/Yb)_N$ = 87.01-120.34), with moderate to high fractionation of light and heavy rare earth elements ($(La/Sm)_N$ = 3.63-7.96; $(Gd/Yb_{)N}$ = 7.81-12.88), and strong negative Eu anomaly (Eu*/Eu = 0.17) (Figure 11c').

In the granite typology classification diagrams (Whalen et al. 1987), the Sant'Ana Granodiorite samples plot in the fields of A-type granites and I-S-type fractionated granites (Figure 12a-d). In the FeOt/(FeO_t+MgO) versus Al_2O_3 diagram from Dall'Agnol and Oliveira (2007), the samples are classified between the fields of oxidized and calc-alkaline A-type granites (Figure 12e). The samples plot mainly in syn- to post-collisional granite fields regarding the tectonic environment (Figures 13a-d; Pearce et al. 1984; Pearce 1996).

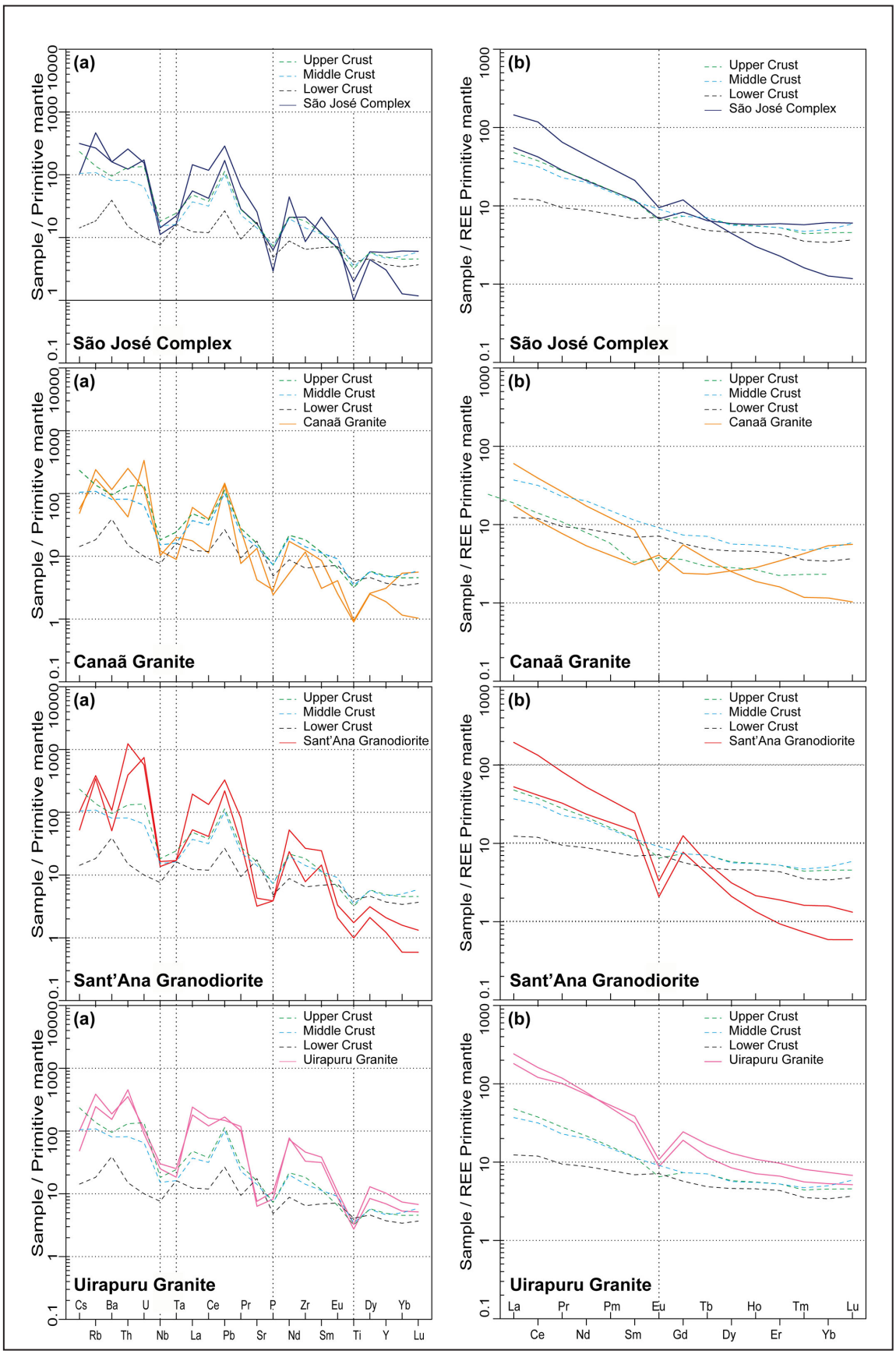

FIGURE 11 – Diagram of trace elements and rare earths for the granitoids under study. (11a)-(11b)-(11c)-(11d) Trace element diagram normalized to the primitive mantle (right-hand side); (11a')-(11b')-(11c')-(11d') Rare earth element diagram normalized to the mantle (right-hand side), the values with the mantle values from McDonough and Sun (1995).

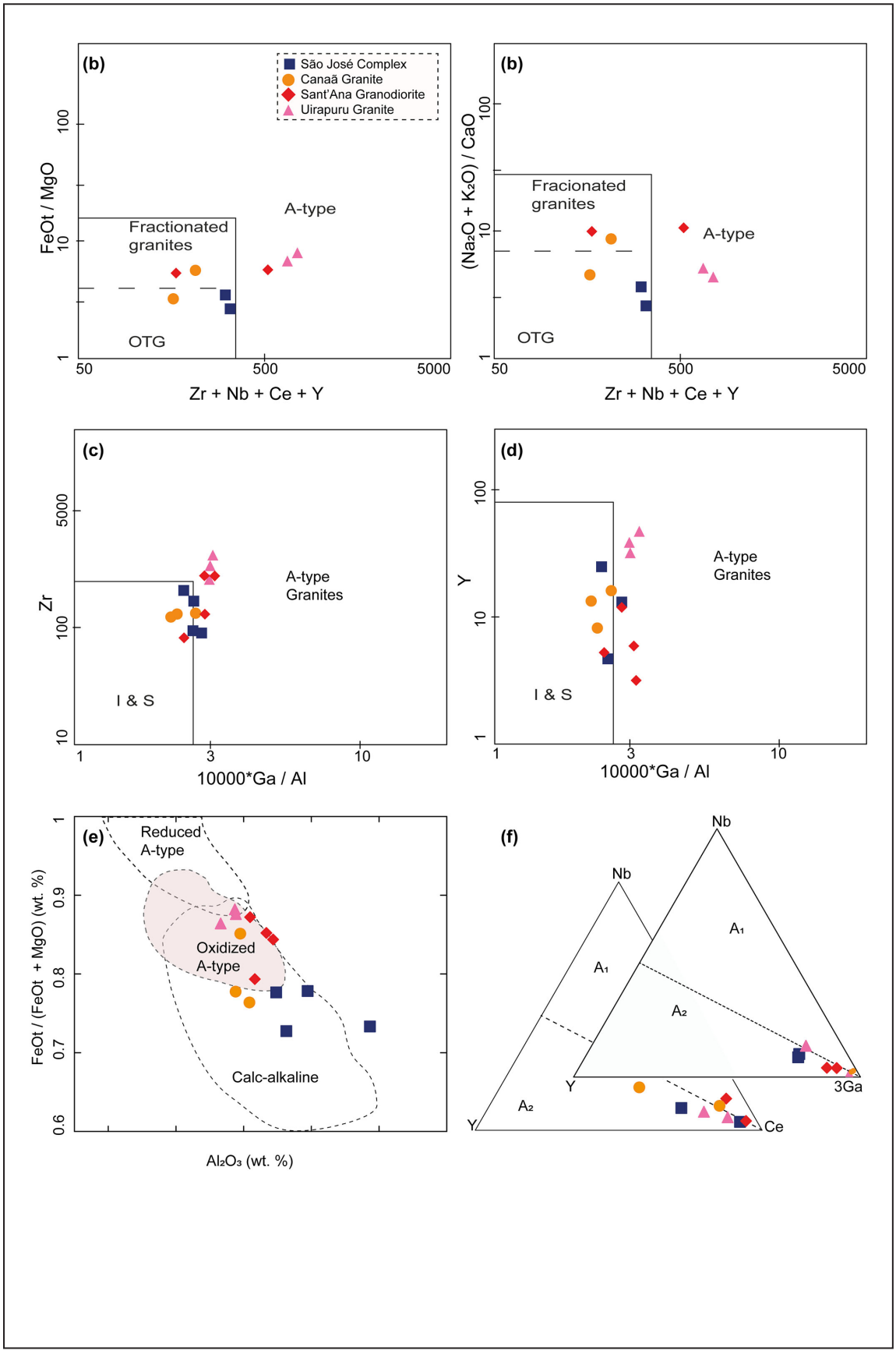

FIGURE 12 – Classification diagrams for the granitoids of the northwestern region of the Bacajá domain. (a-b-c-d) Discriminant diagrams for granite typology classification by Whallen et al. (1987): OTG = Unfractioned Granites; (e) discriminant diagram $FeO_t/(FeO_t+MgO)$ versus Al_2O_3 for classification between calci-alkaline and reduced and oxidized type-A granites by Dall'Agnol and Oliveira (2007); (f) ternary diagrams for A-type granite classification (Eby 1992).

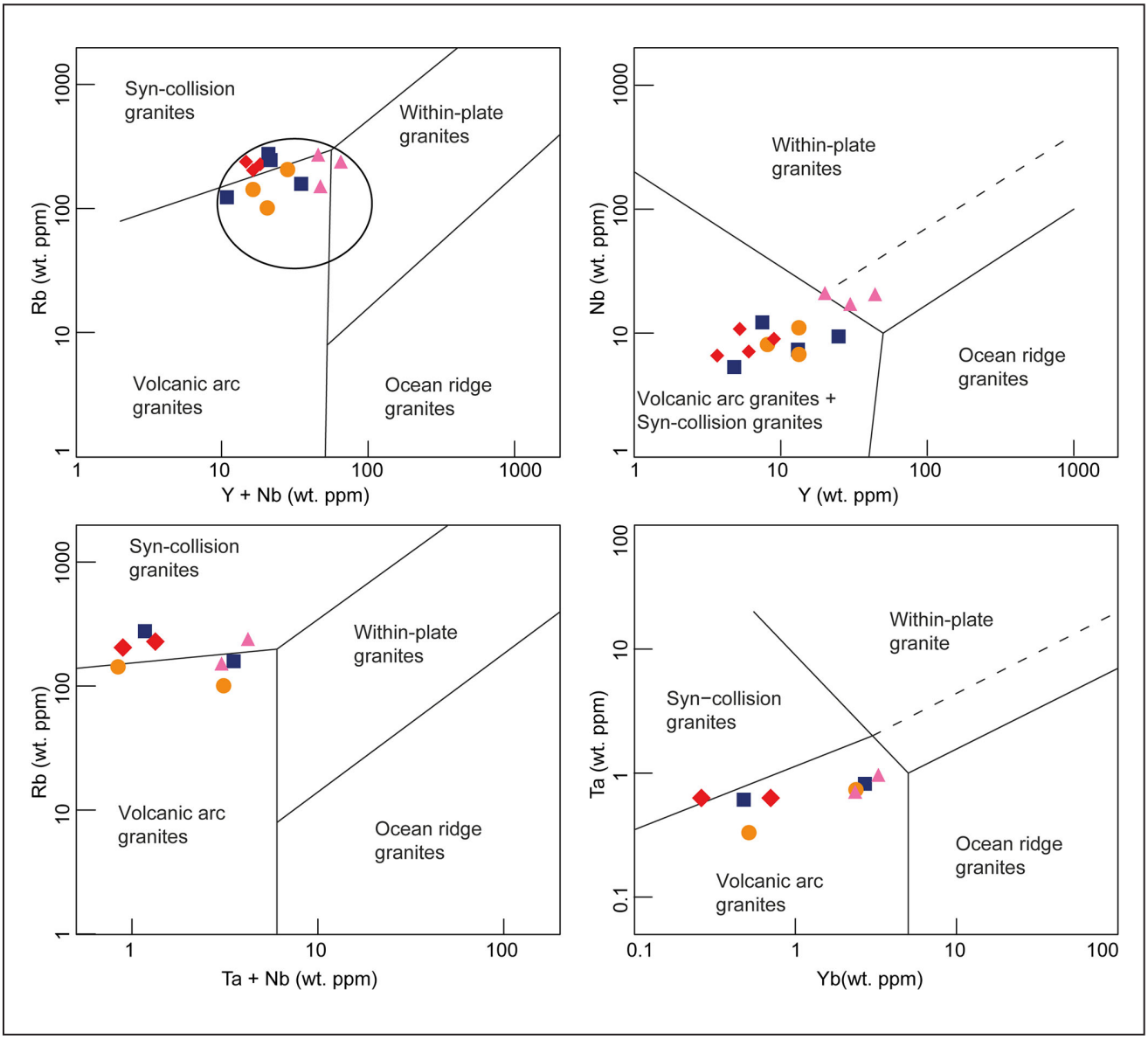

FIGURE 13 – Tectonic discrimination diagrams for the granites of the northwestern region of the Bacajá Domain. (13a)-(13b)-(13c)-(13d) Tectonic discrimination diagrams of granites from Pearce et al. (1984) with the post-collisional granite field from Pearce (1994).

4.2.4. Uirapuru Granite

Three samples of Uirapuru Granite (CVM-31, CVM-36, CVM-38) were analyzed. They have SiO_2 content varying from 68.89 to 71.43 wt% and plot in the granite field (Figure 10a; Debon and Le Fort 1983). They are slightly peraluminous to metaluminous (A/CNK = 0.98-1.10; Figure 10b). In the K_2O versus SiO_2 diagram (Peccerillo and Taylor 1976), all samples plot in the shoshonitic series (Figure 10c). Using the $(Al_2O_3 + CaO) / (FeOt + Na_2O + K_2O)$ versus $100 (MgO + FeOt + TiO_2) / SiO_2$ diagram from Sylvester (1989), the analyzed samples are classified as alkaline granites (Figure 10d).

All the samples are characterized by restricted K_2O content (5.49-5.68 wt%), K_2O/Na_2O ratios (2.05-2.18), $A_{l2}O_3$ content (13.32-13.77 wt%), CaO (1.16-2.05%), MgO (0.44-0.61%), Na_2O (2.52-2.73 wt%) and Fe_2O_3 (3.11-44.49 wt%), showing negative correlations between SiO_2 content versus FeOt, CaO, and P_2O_5 (Figure 8).

In the $FeO_t/(FeO_t+MgO)$ versus SiO_2 diagram from Frost et al. (2001), the samples plot in the field of ferrous granites (Figure 10e) with low Mg# values (19.24-21.89) and high values of $FeO_t/(FeO_t+MgO)$, between 0.86 and 0.88.

In the multielement diagram of trace elements normalized to the mantle (McDonough and Sun 1995), the samples of Uirapuru Granite are enriched in Rb, Th, U, La, Ce, Pb, Nd, Zr, Sm, Dy; depleted in Ba, Nb, Ta, Sr and P and Ti (Figure 11d). They exhibit low to moderate Sr (126-151 ppm) and Rb (147-260 ppm) content, with moderate to high K/Rb ratios (215.77-373.52 ppm), high Rb/Sr ratio (1.17-1.94), low Rb/Ba ratio (0.15-0.28), moderate to high Sr/Y ratio (3.44-6.12) (Table 2).

The sum of rare earth elements is high (487.13 to 591.14 ppm). In the mantle normalized diagram for rare earth elements (McDonough and Sun 1995), the two analyzed samples exhibit a strong negative Eu anomaly (Eu*/Eu = 0.33) (Figure 11d'), are enriched in light rare earth elements

relative to heavy rare earth elements (La/Yb from 23.95 to 44.30), exhibit moderate to high fractionation of light and heavy rare earth elements ($(La/Sm)_N$ = 4.70-7.61; $(Gd/Yb)_N$ = 3.25-3.53).

In the granite classification diagrams (Whalen et al. 1987), the samples of the Uirapuru Granite plot in the field of A-type granites (Figure 12a-d). This classification is confirmed by the $FeO_t/(FeO_t+MgO)$ versus Al_2O_3 diagram by Dall'Agnol and Oliveira (2007), in which the rocks fall into the oxidized A-type granites (Figure 12e) and by the Eby (1992) diagram in which the samples are classified in the field of A2-subtype granites (Figure 12f). Regarding the discrimination of the tectonic environment, the samples plot in a transitional field among syn-collisional, within plate and volcanic arc environments (Figures 13a-d; Pearce et al. 1984; Pearce 1996).

4.3. U-Pb geochronology in zircon

Data from zircon U-Pb analyses are presented in Tables 2 and 3. Two samples were analyzed by LA-ICP-MS, a biotite tonalite (CVM-33) from the São José Complex, and a biotite monzogranite (CVM-22) belonging to the Sant'Ana Granodiorite.

4.3.1. São José Complex (CVM-33)

The analyzed sample corresponds to medium-grained biotite tonalite (Figure 14a). The zircon crystals analyzed in the CVM-33 sample have lengths ranging from 100 to 160 µm and widths of 60 and 100 µm, exhibiting a color ranging from transparent to light yellow, with euhedral to subhedral shapes. They are elongated and rounded prismatic crystals with weak concentric oscillatory zoning. Some crystals have micro-inclusions. In general, the crystals show low luminescence overgrowth. The cathodoluminescence images of the analyzed zircon crystals and their respective spots are shown in Figure 14b.

Altogether fourteen zircon crystals were analyzed in the CVM-33 sample. They have U contents ranging from 143-600 ppm, Th between 11-254 ppm and Th/U ratios ranging from 0.42 to 0.84 (Table 3). 4 crystals allowed the calculation of a concordia age (Fig. 14c), indicating 2501 ± 4 Ma (MSWD = 0.13). A discordia line was also made with eight zircon crystals that showed an age of 2502 ± 6 Ma; MSWD = 2.9 (Fig. 14d). All the analyzed domains reveal Th/U >0.1 and are therefore interpreted as crystallization ages. A zircon crystal with an age of 2594 ± 16 Ma was considered to be inherited from a protolith from a Neoarchean source (Table 3).

4.3.2. Sant'Ana Granodiorite (CVM-21)

The analyzed sample corresponds to medium-grained monzogranite biotite (Figure 15a). The analyzed zircon crystals from the CVM-21 sample have lengths ranging from 150 to 200 µm and widths from 50 to 100 µm, ranging from colorless to yellow, with euhedral to subhedral shapes. They are elongated, rounded prismatic crystals with weak concentric zonation and exhibit microfractures. They show fractured and altered cores, and oscillatory or convolute rims.

The cathodoluminescence images of the analyzed zircon crystals and their respective spots are shown in Figure 15b. Twenty zircon crystals were analyzed in sample CVM-21. They have U content between 246 to 967 ppm, Th content between 14 to 1890 ppm and Th/U ratios are between 0.03 to 2.17 (Table 4).

A discordia with seven zircon crystals was calculated (Figure 15c), indicating an age of 2124 ± 7 Ma at the upper intercept (MSWD = 5.2). The Th/U ratios of the concord crystals mostly range from 0.42 to 0.82 and the age is interpreted as crystallization age.

5. Discussion

5.1. Petrogenetic classification

5.1.1. São José Complex

The analyzed rocks of the São José Complex are slightly meta- to peraluminous with medium to high-K calc-alkaline affinities. They exhibit calc-alkaline and strongly peraluminous affinities to highly fractionated calc-alkaline. The São José Complex has A/CNK ratios < 1.1, exhibits high and low magnesium values, high Na_2O content, and a negative correlation between P_2O_5 and SiO_2. In addition to these features, the relatively low HSFEs (308-326 ppm), and rare earth elements (161-385 ppm), suggest affinity for calc-alkaline I-type granites (e.g., White 1979; Whalen et al. 1987; Chappel 1999; Clemens 2003; Chappell et al. 2012).

5.1.2. Canaã Granite

The Canaã Granite samples are slightly metaluminous to peraluminous with high-K calc-alkaline to shoshonitic affinities. They range from calc-alkaline and strongly peraluminous to highly fractionated calc-alkaline, exhibiting high Na_2O and K_2O and low A/CNK < 1.1. Together, the trace and rare-earth elements patterns, such as mild negative Eu anomalies, low sum of rare earth elements (49-142 ppm), and HFSE contents (161-212 ppm), indicate that Canaã Granite is geochemically similar to high-K calc-alkaline I-type granites (e.g. Chappell 1999).

Some samples from Canaã Granite preserve supracrustal xenoliths of biotite gneisses, which are important features that occur in S-type granites (e.g., Clemens 2003). However, such Canaã Granite samples do not exhibit other aluminum-rich minerals such as muscovite, garnet, cordierite and sillimanite. As the biotite was the only strongly peraluminous phase identified, it was not possible to confirm the affinity with classical S-type granites.

5.1.3. Sant'Ana Granodiorite

The Sant'Ana Granodiorite is a slightly meta- to peraluminous unit with high-K calc-alkaline affinity to shoshonitic, containing similar relations with calc-alkaline to alkaline rocks. The samples have high SiO_2 content, total alkali (K_2O + Na_2O), Ga/Al ratio greater than 2.6, and a high sum of rare earth elements in two samples like A-type granites (e.g., Loiselle and Wones 1979; Whalen et al. 1987; Nardi and Bitencourt 2009; King et al. 2001). However, two other samples show low concentrations of Zr (82-140 ppm) and HSFE (Zr + Ce + Nb + Y < 350 ppm), which indicate affinities with I-type granites. These affinities are corroborated in the granite classification diagrams, where the samples plot both in the fields of fractionated I-S- and A-type granites (Fig. 12a-d; Whalen et al. 1987).

TABLE 3 – Zircon U-Pb LA-ICP-MS data - São José Complex (Sample CVM-33)

Zircon	Spot	f206	U		Th		Pb		Th/U	$^{206}Pb/^{204}Pb$	$^{207}Pb/^{235}U$	2σ	Concordia data				Rho	$^{207}Pb/^{206}Pb$		Ages (Ma)[1]		$^{207}Pb/^{235}U$	2s	$^{208}Pb/^{232}Th$	2σ	% conc[2]
													2σ%	$^{206}Pb/^{238}U$	2s	2σ%			2s	$^{206}Pb/^{238}U$	2s					
		(%)	(μg.g^{-1})	2σ	(μg.g^{-1})	2 σ	(μg.g^{-1})	2 σ	Calculated																	
1	Spot83.FIN2	0.04	148	4	63	1	97	3	0.42	44500	9.84	0.200	2.0325	0.427	0.009	2.1561	0.53	2528	19	2290	41	2416	18	2370	290	91
2.1	Spot84.FIN2	0.03	237	5	113	2	136	4	0.48	69800	9.34	0.220	2.3555	0.419	0.012	2.8640	0.66	2496	20	2248	55	2367	21	2150	180	90
3.2	Spot87.FIN2	0.03	274	7	115	2	110	3	0.42	56650	6.22	0.130	2.0900	0.300	0.008	2.5376	0.58	2347	22	1688	38	2007	18	1770	150	72
5	Spot90.FIN2	0.05	143	2	117	2	132	3	0.82	40300	9.81	0.170	1.7329	0.431	0.009	1.9944	0.60	2513	16	2302	39	2411	16	2260	130	92
6	Spot91.FIN2	0.03	186	6	106	4	121	6	0.57	60300	11.82	0.240	2.0305	0.495	0.012	2.4242	0.66	2594	17	2580	51	2587	19	2160	180	99
7	Spot92.FIN2	0.04	167	4	106	2	123	4	0.63	50350	10.40	0.250	2.4038	0.464	0.013	2.8017	0.70	2496	21	2448	56	2472	22	2280	160	98
11	Spot97.FIN2	0.04	167	11	117	8	140	10	0.70	48150	10.54	0.160	1.5180	0.472	0.008	1.7782	0.59	2497	14	2491	37	2481	14	2380	220	100
12	Spot98.FIN2	0.03	245	12	130	5	172	8	0.53	68600	10.45	0.220	2.1053	0.465	0.011	2.3656	0.65	2506	17	2457	47	2479	19	2530	120	98
17	Spot104.FIN2	0.06	191	9	149	7	87	5	0.78	30150	5.80	0.160	2.7586	0.259	0.008	3.0948	0.62	2497	24	1479	41	1934	24	980	180	59
19	Spot106.FIN2	1.82	875	19	15	0	108	5	0.02	1025	7.41	0.140	1.8893	0.334	0.008	2.3068	0.68	2441	18	1857	36	2157	17	4000	1300	76
21	Spot108.FIN2	0.03	216	5	149	3	184	5	0.69	59600	11.49	0.240	2.0888	0.456	0.011	2.4123	0.55	2674	20	2415	49	2566	19	2440	120	90
22.1	Spot109.FIN2	0.10	578	14	254	8	35	2	0.44	19000	0.74	0.025	3.3921	0.053	0.002	3.0019	0.59	1659	35	334	10	559	15	157	94	60
22.2	Spot110.FIN2	0.07	600	11	11	0	5	0	0.02	27150	0.89	0.019	2.1445	0.076	0.001	1.7105	0.50	1310	23	471.6	8	646	10	3300	1400	73
23	Spot111.FIN2	0.03	207	5	174	3	188	5	0.84	54750	10.16	0.230	2.2638	0.439	0.011	2.5057	0.63	2540	20	2347	48	2438	21	2260	120	92

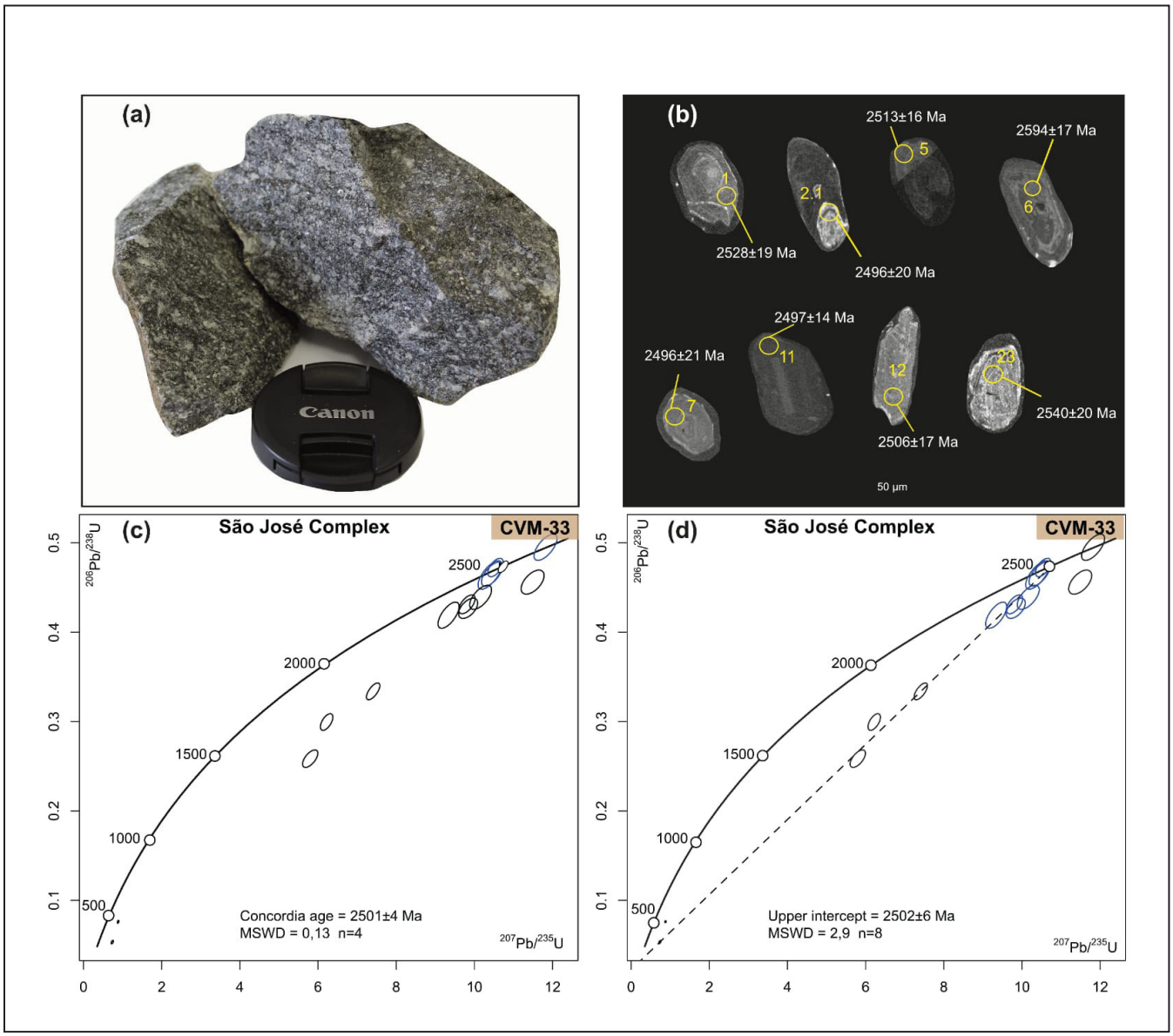

FIGURE 14 – Hand sample, cathodoluminescence images and diagrams used for geochronological studies. (a) Hand sample of the analyzed rock; (b) Cathodoluminescence images of zircon crystals from the São José Tonalite (Sample CVM-33). Spot size: 25 µm; (c) Concordia diagram with concordant analyses for the zircon of sample CVM-33; (d) Concordia diagram with discordant analyses for the zircon of sample CVM-33.

5.1.4. Uirapuru Granite

The samples of Uirapuru Granite are slightly meta- to peraluminous with shoshonitic affinity in the diagram of Peccerillo and Taylor (1976) and/or alkaline in the classification of Sylvester (1989). They exhibit high total alkali content (K_2O +Na_2O = 8.01-9.70), high FeO_t / ratios (FeO_t + MgO = 0.86-0.88, greater than 0.85), high FeO_t/MgO ratios (6.36-7.48), Ga/Al ratios greater than 2.6 (2.94-3.22) and Nb enrichment (16-20 ppm). Moreover they have high HSFE (Zr +Nb + Ce + Y = 520-750 ppm), high sum of rare earth elements (456-591 ppm) and depletion in Ba, Sr, Eu, which are characteristics that suggest affinity with A-type granites (e.g., Loiselle and Wones 1979; Whalen et al. 1987; Eby 1992; Nardi and Betencourt 2009; King et al. 2001).

The granite classification diagrams of Whalen et al. (1987) also suggested an affinity of the Uirapuru Porphyritic Granite with A-type granites. It is hypothesized that it also confirmed the criteria of the diagram by Dall'Agnol and Oliveira (2007), that classify granites in calcium-alkaline and A-type oxidized versus reduced, as shown above, the samples plot in the field of oxidized A-type granites. The Uirapuru Porphyritic Granite shows high Y/Nb and Yb/Ta ratios and is classified as A2-subtype granites, which are formed in post-collisional settings by the melting of continental sources (Eby 1992).

5.2. Tectonic Setting

High-K calc-alkaline I-type granites are usually formed during the transition from a compressional to an extensional tectonic setting (e.g., Barbarin 1999; Zhu et al. 2015). The strong negative anomalies of Nb, Ta, P and Ti present in the granitoid samples are typical of magmas generated in an arc setting via subduction processes (e.g., Pearce and

Table 4 – Zircon U-Pb LA-ICP-MS data - Sant'Ana Granodiorite (Sample CVM-21)

Zircon	Spot	ƒ206	U		Th		Pb		Th/U	$^{206}Pb/^{204}Pb$	$^{207}Pb/^{235}U$	2σ	Concordia[1] data		2σ	2σ%	Rho	$^{207}Pb/^{206}Pb$		Ages (Ma)[1]		$^{207}Pb/^{235}U$	2σ	$^{208}Pb/^{232}Th$	2σ	% conc[2]
													2σ%	$^{206}Pb/^{238}U$						$^{206}Pb/^{238}U$						
		(%)	(μg.g^{-1})	2σ	(μg.g^{-1})	2σ	(μg.g^{-1})	2σ	Calculated																	
1	Spot113.FIN2	2.38	402	11	266	7	335	10	0.66	787	6.50	0.230	3.5385	0.33	0.014	4.2296	0.74	2276	24	1819	67	2033	33	2350	120	80
3	Spot115.FIN2	13.41	967	26	1890	190	496	15	1.95	139	1.70	0.037	2.1765	0.06	0.002	2.8169	0.54	2808	25	399	11	1008	14	709	73	40
4.1	Spot116.FIN2	6.81	700	24	199	4	361	10	0.28	274	2.50	0.088	3.5271	0.11	0.005	4.0650	0.75	2551	22	673	26	1266	25	2930	160	53
5	Spot118.FIN2	0.19	530	10	1149	33	305	12	2.17	9740	0.49	0.014	2.8513	0.03	0.001	2.1985	0.32	1958	32	190.6	4.1	406.3	9	599	27	47
6.1	Spot119.FIN2	2.16	235	9	147	4	200	9	0.63	867	6.62	0.290	4.3807	0.34	0.018	5.2478	0.66	2304	35	1855	84	2045	41	2440	150	81
6.2	Spot120.FIN2	5.70	943	36	119	6	281	12	0.13	328	3.11	0.140	4.5016	0.14	0.007	5.2113	0.62	2522	37	849	41	1425	35	2540	330	60
7	Spot121.FIN2	5.84	246	8	268	6	469	16	1.09	320	8.99	0.220	2.4472	0.39	0.011	2.8424	0.61	2599	24	2079	52	2330	22	2830	110	80
8	Spot123.FIN2	2.43	715	15	14	0	205	9	0.02	768	4.38	0.120	2.7397	0.23	0.008	3.3703	0.54	2242	27	1305	40	1697	23	14300	1100	58
9.1	Spot124.FIN2	7.67	470	12	13	1	330	10	0.03	244	3.82	0.088	2.3055	0.17	0.006	3.3193	0.70	2573	22	985	30	1588	18	21100	1100	62
9.2	Spot125.FIN2	6.52	944	15	54	2	306	7	0.06	287	1.79	0.033	1.8456	0.09	0.002	2.1954	0.63	2271	16	561	12	1041	12	6550	420	54
10	Spot126.FIN2	8.01	452	23	575	28	732	42	1.27	234	5.77	0.150	2.5997	0.24	0.007	2.9499	0.69	2635	23	1370	36	1939	22	1961	82	52
13	Spot128.FIN2	4.47	633	21	56	2	263	10	0.09	418	3.84	0.120	3.1250	0.17	0.006	3.4364	0.77	2440	20	1032	33	1589	25	5760	500	65
15	Spot130.FIN2	0.03	422	12	130	3	123	4	0.31	61500	4.40	0.085	1.9318	0.25	0.006	2.2240	0.69	2082	17	1421	28	1711	16	1850	130	68
16	Spot131.FIN2	5.20	458	11	239	6	201	6	0.52	360	2.40	0.051	2.1277	0.11	0.003	2.3508	0.53	2415	22	678	15	1237	15	1360	100	55
17	Spot132.FIN2	0.04	261	5	244	6	228	7	0.93	44950	5.31	0.110	2.0716	0.29	0.006	2.2401	0.61	2175	19	1618	32	1868	17	1779	86	74
18.2	Spot134.FIN2	0.02	532	22	258	7	330	13	0.48	117550	7.30	0.160	2.1918	0.41	0.010	2.4213	0.71	2104	17	2216	47	2148	20	2255	75	105
19	Spot135.FIN2	8.37	440	10	511	9	434	11	1.16	223	3.59	0.083	2.3107	0.15	0.004	2.5777	0.67	2593	20	907	22	1545	18	1351	63	59
20.1	Spot136.FIN2	0.98	544	27	93	4	204	8	0.17	1899	8.35	0.140	1.6766	0.45	0.009	1.9486	0.64	2152	16	2398	39	2270	15	3110	240	111
21	Spot138.FIN2	0.04	312	8	29	1	72	3	0.09	45000	4.67	0.120	2.5696	0.25	0.007	2.8129	0.70	2176	22	1412	35	1760	21	3500	650	65
22	Spot139.FIN2	0.02	377	9	112	2	121	4	0.30	85950	7.11	0.160	2.2504	0.39	0.010	2.5359	0.68	2103	19	2126	46	2123	19	2410	170	101

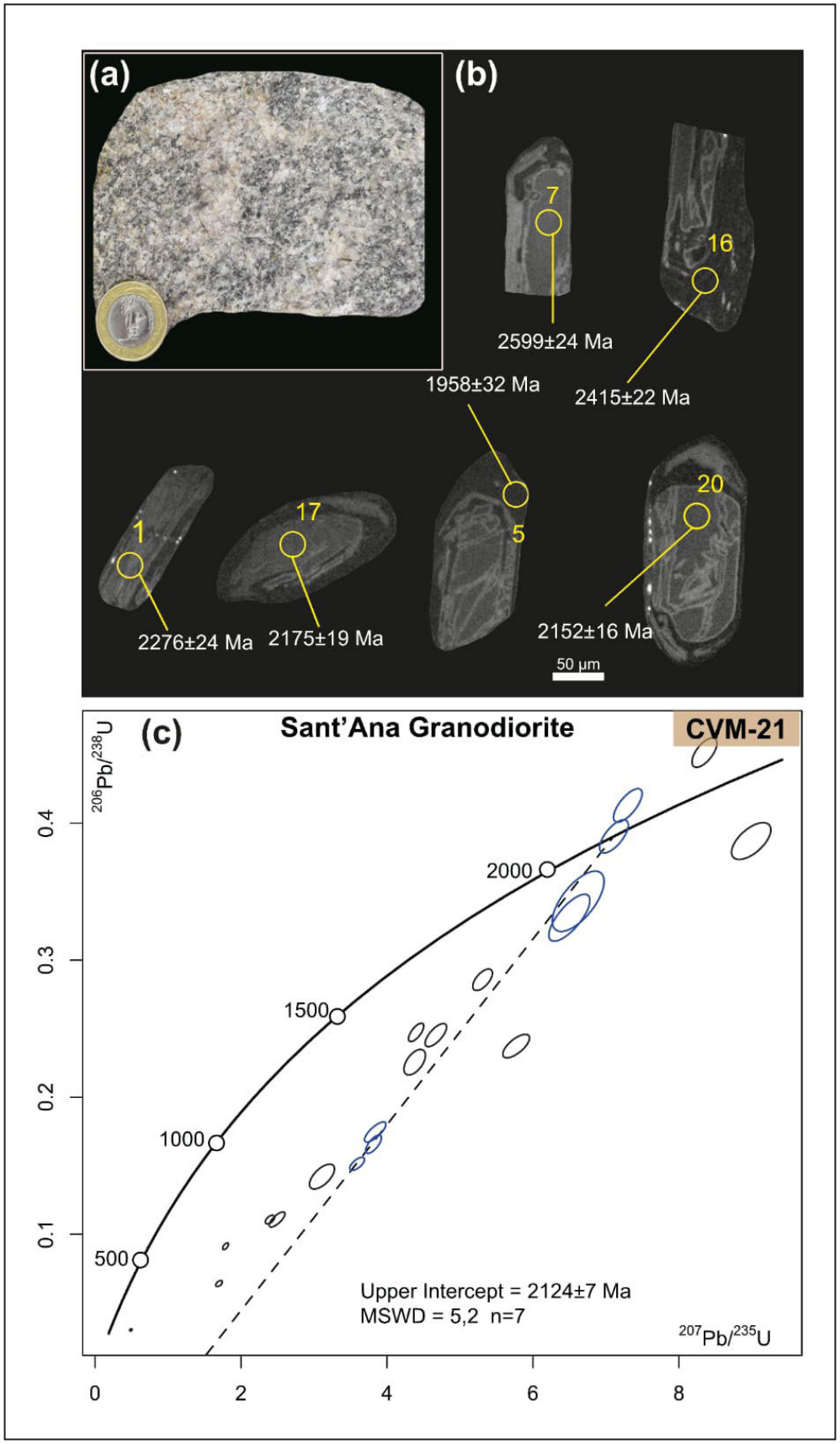

FIGURE 15 – Hand sample, cathodoluminescence images and diagrams used for geochronological studies. (a) Hand sample of the analyzed rock; (b) Cathodoluminescence images of the zircon crystals from the Sant'Ana Granodiorite (Sample CVM-21). Spot size: 25 µm; (c) Concordia diagram with concordant analyses for the zircon crystals from sample CVM-21

Peate 1995; Schandl and Gorton 2002). Furthermore, the rocks exhibit low concentrations of Nb and Ga, similar to the values of calc-alkaline granitoids of normal magmatic arcs (Brown et al. 1984).

The negative anomalies in the Nb-Ta pair may indicate that these granitoids were produced by the chemical differentiation of arc-derived magmas, with continental crust involvement, indicating that the magmas derived or interacted with materials from the upper crust (e.g., Zartman and Doe 1981; Saunders et al. 1991; Klein et al. 2012).

In the tectonic discrimination diagrams, the granites of the São José Complex exhibit chemical characteristics compatible with pre- to syn-collisional arc environments. In comparison, the Canaã Granite and Uirapuru Granite have characteristics that are more compatible with those of syn- to post-collisional environments with some plotting in intraplate settings.

Granitoids related to volcanic arcs can vary their tectonic configuration from oceanic to continental, which leads to changes in geochemical and mineralogical characteristics. Granites associated with primitive tholeiitic oceanic arcs are dominated by quartz diorite and tonalite. In contrast, granites related to arcs of active continental margins are dominated by quartz monzonite, granodiorite and granite belonging to the high-K calc-alkaline and shoshonitic series (Pearce et al. 1984).

In our rocks, shoshonitic and alkaline associations predominate, constituted mainly by monzogranites, granodiorites, of predominantly ferrous character in Canaã Granite, Sant'Ana Granodiorite and Uirapuru Granite. However, in the São José Complex there are tonalites with medium to high-K calc-alkaline character associated with amphibolites.

These characteristics, together with the ages obtained for the granitoids of the São José Complex and the Sant'Ana Granodiorite, indicate that these granitoids represent two independent magmatic events. Besides that, it is also inferred that the São José Complex tonalites were generated in a continental arc subduction environment in a pre-collisional setting, while the Granitoids of Canaã Granite, Sant'Ana Granodiorite and Uirapuru Porphyritic Granite may have been formed in a syn- to post-collisional arc environment after an episode of crust thickening.

The variation among fractionated calc-alkaline (Canaã Granite) granites, transitional (Sant'Ana Granodiorite) and alkaline/shoshonitic rocks (Uirapuru Granite), combined with an increase in Nb, attest to a possible increase in the arc maturity (e.g., Brown et al. 1984). This type of association also suggests a post-collision environment (e.g. Wang et al. 2009).

5.3. Regional Correlations

5.3.1. São José Complex

U-Pb zircon geochronological data provided a concordant age of 2501 ± 4 Ma and a discordant age of 2502 ± 6 Ma for the granite of the São José Complex. This age is older than ages related to the Transamazonian cycle. Similar ages (2503 ± 10 Ma and 2487 ± 13 Ma) found in this work were obtained by Santos (2003) and Vasquez (2006), respectively, in orthogneisses from the west of the Bacajá Domain. This area represents a Siderian magmatic arc amalgamated into a Neo-Archaean-Siderian block (Vasquez et al. 2008).

In the southeastern region of the Bacajá Domain, close to the Carajás Domain, Salgado et al. (2019) dated a metagranite with an age of 2549 ± 5.9 Ma (U-Pb) that is interpreted as A-type granite that composes the basement of the Bacajá Domain, probably related to an extensional rift environment. Salgado et al. (2019) also correlate this metagranite with A-type granites from the Carajás Domain, such as the Old Salobo Granite and the Rio Itacaiúnas Granite.

Further north of the Carajás Domain, Toledo et al. (2019) found crystallization ages in a granite of 2557 ± 26 Ma. Although these ages are different from most of those found for Archean granitoids of the Carajás Block (2.7-3.0 Ga; Vasquez et al. 2008; Tassinari et al. 2000), the definition of these Neo-Archaean to Early-Siderian ages within the Bacajá Domain allows speculating about the contribution of an Archean crust from the Carajás Block within the Bacajá Domain.

The contribution of Neoarchean to early-Siderian crust is suggested by geophysical data from satellites combined with interpretations of geochronological data (Motta et al. 2019). These authors indicate that the Carajás and Bacajá Domains may have shared common pre-Transamazonian Cycle evolution. From the Transamazonian cycle forward, they have a different evolution with additions of juvenile crust in the Bacajá Domain up to 2.0 Ga, associated with a later crustal reworking. However, it is still necessary to specify the degree of contribution of a probable Archean crust of Carajás in the Bacajá Domain.

5.3.2. Sant'Ana Granodiorite

A sample of the Sant'Ana Granodiorite was dated and presented a discordant age of 2124 ± 7 Ma, which is similar to those found in the Bacajá Domain, which are associated with the Tapiranga Metatonalite rocks (2133 Ma; Vasquez 2006), or also to the Bacajaí Complex (2114 ± 33 Ma; Faraco et al. 2005; Monteiro 2006). Considering the analytical error, these ages are interpreted as representing the collisional phase of a Rhyacian magmatic arc (2.21-2.18 Ga), probably formed during the Transamazonian Cycle (Vasquez et al. 2008).

There are Rhyacian granitoid suites in the Guiana Shield, such as the Papa Vento Intrusive Suite with ages of 2136 ± 8 - 2138 ± 20 Ma, that is interpreted as calc-alkaline arcs (Rosa-Costa et al. 2014; Vianna et al. 2020). The Bacajá Domain and the Guiana Shield terrains are chrono-correlated during the Transamazonian Cycle. A younger age was obtained for a monzogranite belonging to the Sant'Ana Granodiorite (2124 ± 7 Ma) that exhibits shoshonitic affinity. It is suggested t that its formation is related to a late- to a post-collisional tectonic configuration of the Transamazonian Orogeny.

5.4. Sources of the magmatic associations

Different processes can generate peraluminous granites, including (1) fractional crystallization of low metaluminous phases with metaluminous melts (Wu et al. 2003); (2) dehydration melting of quartz amphibolite (Patiño Douce and Beard 1995); (3) vapor-absent or water-saturated melting of aluminum-rich metapelites or metagrawakes (Le Breton and Tompson 1988; Patiño Douce and Johnston 1991; Patiño Douce and Beard 1995) and (4) partial melting from mixing of metasedimentary to basaltic rocks (Skjerlie and Johnston 1992; Patiño Douce 1995).

Usually, the granites analyzed herein exhibit high SiO2 and low MgO contents. These characteristics suggest that crust-derived or highly fractionated magmas were their sources (e.g., Liu 2018). Granitoids exhibit negative Ti, Sr, Nb and P anomalies that may reflect the fractionation of minerals such as biotite, ilmenite, and apatite. Negative Nb and Ti anomalies are also interpreted as reflecting different factors such as (1) contamination of magma and/or its source with crustal components; (2) interaction between magma and a depleted peridotite; (3) amphibole fractionation (Martins 1987). In our rocks, it is suggested that these anomalies are mainly derived from crustal components, which is reinforced by Nd isotope data from Macambira et al. (2004). This hypothesis is also supported by the presence of positive anomalies of Rb, Th, Ce and Sm, as well as negative anomalies of Y, attributed to the strong involvement of crustal materials in the source of magmas (e.g., Pearce et al. 1984)

Our granites have Rb/Sr ratios lower than four, suggesting that their magmas were generated under vapor-present conditions (e.g., Harris et al. 1993). In addition, the low MgO of most samples combined with the low Rb/Sr ratios may also indicate the contribution of biotite during the production of these granitoids.

The strong negative anomalies of Eu, and Sr and Ba depletion in Sant'Ana Granodiorite and Uirapuru Granite suggest extensive plagioclase and/or K-feldspar fractionation, indicating a fractionation sequence controlled by feldspars and biotite (e.g., Rollinson 1992). Plagioclase fractionation can occur due to partial melting of rocks from basaltic to intermediate compositions, producing negative Eu anomalies and Sr depletion (Landenberger and Collins 1996).

A sample from Canaã Granite exhibits positive Eu anomaly and enrichment of heavy rare earth elements. K-feldspar accumulation can explain the positive Eu anomaly under high-temperature conditions. This mineral incorporates more Eu than under low-temperature conditions (e.g., Bea et al. 1994). Granitic rocks with positive Eu anomalies and low concentrations of light rare earth elements have been recorded in granitic terrains. These characteristics are generally associated with migmatites and interpreted as generated by the partial melting of pelitic metasedimentary rocks (e.g., Jung et al. 2001).

Experimental petrological studies have shown that amphibolitic/basaltic lower continental crust melts are characterized by low Mg# (<40) irrespective of the degree of partial melting. In contrast, those with high Mg# value can be generated by involvement with mantle components (Rapp and Watson 1995). In this study, the Canaã Granite, Sant'Ana Granodiorite and Uirapuru Granite rocks exhibit low Mg# (19-31) and low MgO (0.25-0.7 wt%), which may indicate their origin by the melting of crustal magmas without a significant contribution of mantle magmas. However, two samples from the São José Complex exhibit higher Mg# (33-40) and MgO (1.16-1.45 wt%), in addition to high CaO (2.64-4.57 wt%) and mafic xenoliths (Figure 4a), that may indicate mixing of crustal magmas from the lower crust with mantle magmas.

The ages obtained for the granitoids of the São José Complex and Sant'Ana Granodiorite indicate that independent and distinct magmatic episodes formed these units. Thus, it is suggested that the granitoids from the São José Complex were generated by the partial melting of amphibolitic and/or basaltic sources. In contrast, the Canaã and Sant'Ana units were generated by decompression melting of intermediate rocks from the lower crust after thickening, without mantle material involved. It was also indicated by the high content of SiO_2 and K_2O, resulting in magmas with shoshonitic affinities (e.g., Pitcher 1987).

The Uirapuru Granite exhibits a similar affinity to A-type granites. It has strong negative Eu anomalies, which are usually explained by the fractional crystallization of accessory phases and plagioclase in the presence of a liquid phase (Williamson et al. 1996; Jung et al. 2001). Furthermore, the strong Eu anomaly associated with the high content of Y (21-44 ppm) and microperthitic feldspar in the samples suggest that the primary melt was crystallized at pressures below that of garnet stability by partial melting at shallower depths than 8 kbar and high temperature (e.g., Rapp and Watson 1995; King et al. 1997; Zhang et al. 2011).

There is great divergence regarding the origin of A-type granites, the three main petrogenetic models for the generation of these granites include: (1) differentiation of mafic magmas derived from the mantle (Eby 1990; Turner et al. 1992; Bonin 1996; Bonin 2007) (2) partial melting of crustal rocks (Collins et al. 1982; Frost and Frost 2011; Dall'Agnol et al. 2012), and (3) mixing between mantle-derived mafic magmas and crust-derived magmas (King et al. 1997; Yang et al. 2005; Martin 2006).

Multielemental diagrams of the Uirapuru Granite also exhibit high negative Nb anomalies characteristic of continental crust and may represent the involvement of crustal material in magmatic processes (Rollinson 1993). Additionally, the samples have high Rb/Sr, Rb/Ba ratios, and low Sr/Ba ratios, typical of crustal granites (Harris and Inger 1992).

The chemical composition of the Uirapuru Granite is similar to that of the oxidized A-type granites. In this case, the sources are quartz-feldspathic igneous protoliths (e.g., gneisses of tonalitic composition). Contrasting, sedimentary or basaltic composition will produce reduced granites (Frost et al. 1997; Dall'Agnol et al. 1999; Dall'Agnol and Oliveira 2007). Patiño Douce (1997) carried out an experimental study with rocks from the Sierra Nevada Batholith, in which the low pressure and high temperature melting of tonalite and granodiorite protoliths produced porphyritic A-type metaluminous granites, very similar to those from the Uirapuru Granite. Thus, it is suggested that the Uirapuru Granite originated from the partial melting of the Neoarchean-Siderian lower crustal rocks (basement), such as gneisses of tonalitic or felsic composition (e.g., paragneisses and ortho-granulites that occur in the region).

6. Conclusions

Field data, petrography, geochemistry, and geochronology helped us characterize four granitoid units in the study area: São José Complex, Canaã Granite, Sant'Ana Granodiorite, and Uirapuru Granite.

(1) The São José Complex comprises biotite tonalites slightly peraluminous, medium to high-K calc-alkaline, predominantly ferrous with I-type granite affinities. One U-Pb zircon age of 2501 ± 6 Ma suggests that this granitoid was formed in a pre-collisional continental arc amalgamated to an Archean terrain.

(2) The Canaã Granite comprises biotite monzogranites and tonalites slightly peraluminous, shoshonitic, ferrous with I-type granite affinity, most likely formed in a syn-collisional continental arc tectonic setting related to the Transamazonian Orogeny.

(3) The Sant'Ana Granodiorite is constituted by biotite monzogranites and biotite granodiorites slightly peraluminous, shoshonitic, and ferrous. These rocks exhibit affinities with I- and A-type granites. One sample was dated and presented the age of 2124 ± 6 Ma, suggesting its formation in a continental arc setting in a syn to post-collisional phase.

(4) The Uirapuru Granite is constituted of biotite syenogranites, monzogranites with subordinate tonalites, shoshonitic and/or alkaline, ferrous with an affinity of oxidized A-type granites of the A2-subtype. It may have been formed in a post-collisional tectonic setting at the end of the Transamazonian Orogeny.

(5) It is suggested that the magma source from the granitoids is related to the partial melting of crustal components. However, the source of the granites in the São José Complex may be more related to the partial melting of amphibolitic to metabasaltic rocks, while the probable sources of the other granitoid might be attributed to tonalitic to granodioritic rocks compositions of the lower continental crust, which in the region are represented by orthogneisses and paragneisses of the Bacajá Domain basement.

Acknowledgments

The authors thank the Institute of Geosciences of the University of Campinas for providing access to infrastructure and financial support for the field campaigns and geochemistry e geochronology analyses. We would like thanks the Federal University of Western Pará (UFOPA), especially grateful to Professors Fabriciana Vieira, Alessandro Braga and Erica Cabral for fieldwork support. CSV thanks the University of Campinas for its social programs. WSA also acknowledges the Brazilian National Research Council (CNPq) for research grant (process. 305263/2020-0).

Authorship credits

Author	A	B	C	D	E	F
CSV	■	■	■	■	■	
WSA	■	■				■
FHS		■	■		■	■

A - Study design/Conceptualization **B** - Investigation/Data acquisition
C - Data Interpretation/ Validation **D** - Writing
E - Review/Editing **F** - Supervision/Project administration

References

Almeida F.F.M., Amaral G., Cordani U., Kawashita K. 1973. The Precambrian evolution of the South American cratonic margin south of the Amazon River. In: Nairn A.E.M., Stehli F.G. (eds.) The South Atlantic. New York, Springer, p. 411-446.

Anderson J.R., Payne J.L., Kelsey D.E., Hand M., Collins A.S., Santosh M. 2012. High-pressure granulites at the dawn of the Proterozoic. Geology, 40(5), 431-434. https://doi.org/10.1130/G32854.1 .

Baker P.E., Rea W.J., Skarmeta J., Caminos R., Rex D.C. 1981. Igneous history of the Andean Cordillera and Patagonian Plateau around latitude 46 S. Philosophical Transactions of the Royal Society of London. Series A, Mathematical and Physical Sciences, 303(1474), 105-149. https://doi.org/10.1098/rsta.1981.0194.

Barbarin B. 1999. A review of the relationships between granitoid types, their origins and their geodynamic environments. Lithos, 46(3), 605-626. https://doi.org/10.1016/S0024-4937(98)00085-1 .

Bea F., Pereira M.D., Stroh A. 1994. Mineral/leucosome trace-element partitioning in a peraluminous migmatite (a laser ablation-ICP-MS study). Chemical Geology, 117(1-4), 291–312. https://doi.org/10.1016/0009-2541(94)90133-3 .

Berman R.G., Sanborn-Barrie M., Stern R.A., Carson C.J. 2005. Tectonometamorphism at ca. 2.35 and 1.85 Ga in the Rae domain, western Churchill Province, Nunavut, Canada: insights from structural, metamorphic and in situ geochronological analysis of the southwestern Committee Bay Belt. The Canadian Mineralogist, 43(1), 409-442. https://doi.org/10.2113/gscanmin.43.1.409 .

Bessoles B. 1977. Géologie de l'Afrique: Le craton ouest Africain. Mémoires du Bureau de Recherches Géologiques et Minières, 88, 1-403.

Bonin B. 1996. A-type granite ring complexes: mantle origin through crustal filters and the anorthosite–rapakivi magmatism connection. In: Demaiffe D. (ed.). Petrology and Geochemistry of Magmatic Suites of Rocks in Continental and Oceanic Crusts. A Volume Dedicated to Professor Jean Michot. Université Libre de Bruxelles, Royal Museum for Central Africa, Tervuren, p. 201–218.

Bonin B. 2007. A-type granites and related rocks: evolution of a concept, problems and prospects. Lithos, 97(1-2), 1-29. https://doi.org/10.1016/j.lithos.2006.12.007 .

Brito Neves B.B., Fuck R.A. 2014. The basement of the South American platform: Half Laurentian (N-NW)+ half Gondwanan (E-SE) domains. Precambrian Research, 244, 75-86. https://doi.org/10.1016/j.precamres.2013.09.020 .

Brito Neves B.B. 2011. The Paleoproterozoic in the South-American continent: diversity in the geologic time. Journal of South American Earth Sciences, 32(4), 270-286. https://doi.org/10.1016/j.jsames.2011.02.004 .

Brown G.C., Thorpe R.S., Webb P.C. 1984. The geochemical characteristics of granitoids in contrasting arcs and comments on magma sources. Journal of the Geological Society, 141(3), 413-426. https://doi.org/10.1144/gsjgs.141.3.0413 .

Chappell B.W. 1999. Aluminium saturation in I-and S-type granites and the characterization of fractionated haplogranites. Lithos, 46(3), 535-551. https://doi.org/10.1016/S0024-4937(98)00086-3 .

Chappell B.W., Bryant C.J., Wyborn D. 2012. Peraluminous I-type granites. Lithos, 153, 142-153. https://doi.org/10.1016/j.lithos.2012.07.008 .

Clemens J.D. 2003. S-type granitic magmas - petrogenetic issues, models and evidence. Earth-Science Reviews, 61(1-2), 1-18. https://doi.org/10.1016/S0012-8252(02)00107-1 .

Collins W.J., Beams S.D., White A.J.R., Chappell B.W. 1982. Nature and origin of A-type granites with particular reference to southeastern Australia. Contributions to mineralogy and petrology, 80(2), 189-200. http://dx.doi.org/10.1007/BF00374895 .

Condie K.C. 2000. Episodic continental growth models: afterthoughts and extensions. Tectonophysics, 322(1-2), 153-162. http://dx.doi.org/10.1016/S0040-1951(00)00061-5 .

Condie K.C., Beyer E., Belousova E., Griffin W.L., O'Reilly S.Y. 2005. U–Pb isotopic ages and Hf isotopic composition of single zircons: the search for juvenile Precambrian continental crust. Precambrian Research, 139(1-2), 42-100. http://dx.doi.org/10.1016/j.precamres.2005.04.006.

Condie K.C., Belousova E., Griffin W.L., Sircombe K.N. 2009a. Granitoid events in space and time: constraints from igneous and detrital zircon age spectra. Gondwana Research, 15(3-4), 228-242. https://doi.org/10.1016/j.gr.2008.06.001 .

Condie K.C., O'Neill C., Aster R.C. 2009b. Evidence and implications for a widespread magmatic shutdown for 250 My on Earth. Earth and Planetary Science Letters, 282(1-4), 294-298. https://doi.org/10.1016/j.epsl.2009.03.033 .

Corrigan D., Pehrsson S., Wodicka N., Kemp E. 2009. The Palaeoproterozoic Trans-Hudson Orogen: a prototype of modern accretionary processes. Geological Society, London, Special Publications, 327(1), 457-479. https://doi.org/10.1144/SP327.19 .

Dall'Agnol R., Oliveira D.C. 2007. Oxidized, magnetite-series, rapakivi-type granites of Carajás, Brazil: implications for classification and petrogenesis of A-type granites. Lithos, 93(3-4), 215-233. https://doi.org/10.1016/j.lithos.2006.03.065 .

Dall'Agnol R., Frost C.D., Rämö O.T. 2012. IGCP Project 510 "A-type Granites and Related Rocks through Time": Project vita, results, and contribution to granite research. Lithos, 151, 1-16. https://doi.org/10.1016/j.lithos.2012.08.003.

Dall'Agnol R., Scaillet B., Pichavant M. 1999. An experimental study of a lower Proterozoic A-type granite from the Eastern Amazonian Craton, Brazil. Journal of Petrology, 40(11), 1673-1698. http://dx.doi.org/10.1093/petrology/40.11.1673 .

Debon F., Le Fort P. 1983. A chemical–mineralogical classification of common plutonic rocks and associations. Earth and Environmental Science Transactions of the Royal Society of Edinburgh, 73(3), 135-149. https://doi.org/10.1017/S0263593300010117 .

Dickinson W.R., Gehrels G.E. 2003. U–Pb ages of detrital zircons from Permian and Jurassic eolian sandstones of the Colorado Plateau, USA: paleogeographic implications. Sedimentary Geology, 163(1-2), 29-66. https://doi.org/10.1016/S0037-0738(03)00158-1 .

Eby G.N. 1990. The A-type granitoids: a review of their occurrence and chemical characteristics and speculations on their petrogenesis. Lithos, 26(1-2), 115-134. https://doi.org/10.1016/0024-4937(90)90043-Z.

Eby, G.N. 1992. Chemical subdivision of the A-type granitoids: petrogenetic and tectonic implications. Geology, 20(7), 641-644. https://doi.org/10.1130/0091-7613(1992)020%3C0641:CSOTAT%3E2.3.CO;2 .

Faraco M.T.L., Vale A.G., Santos J.O.S., Luzardo R., Ferreira A.L., Oliveira M., Marinho P.A.C. 2005. Levantamento geológico da região ao norte da província Carajás. In: Souza V.S., Horbe A.M.C. (coords). Contribuições à Geologia da Amazônia. Belém, SBG-Núcleo Norte, v. 4, p. 16-31.

Frost B.R., Barnes, C.G., Collins W.J., Arculus R.J., Ellis D.J., Frost C.D. 2001. A geochemical classification for granitic rocks. Journal of petrology, 42(11), 2033-2048. https://doi.org/10.1093/petrology/42.11.2033 .

Frost C.D., Frost B.R. 2011. On ferroan (A-type) granitoids: their compositional variability and modes of origin. Journal of petrology, 52(1), 39-53. https://doi.org/10.1093/petrology/egq070 .

Frost C.D., Frost R.B. 1997. Reduced rapakivi-type granites: the tholeiite connection. Geology, 25(7), 647-650. https://doi.org/10.1130/0091-7613(1997)025%3C0647:RRTGTT%3E2.3.CO;2 .

Grenholm M. 2019. The global tectonic context of the ca. 2.27-1.96 Ga Birimian Orogen–Insights from comparative studies, with implications for supercontinent cycles. Earth-science reviews, 193, 260-298. https://doi.org/10.1016/j.earscirev.2019.04.017 .

Grenholm M., Jessell M., Thébaud N. 2019. A geodynamic model for the Paleoproterozoic (ca. 2.27–1.96 Ga) Birimian Orogen of the southern West African Craton–Insights into an evolving accretionary-collisional orogenic system. Earth-science reviews, 192, 138-193. https://doi.org/10.1016/j.earscirev.2019.02.006 .

Gumsley A.P., Chamberlain K.R., Bleeker W., Söderlund U., De Kock M.O., Larsson E.R., Bekker A. 2017. Timing and tempo of the Great Oxidation Event. Proceedings of the National Academy of Sciences, 114(8), 1811-1816. https://doi.org/10.1073/pnas.1608824114 .

Harris N.B.W., Inger S. 1992. Trace element modelling of pelite-derived granites. Contributions to Mineralogy and Petrology, 110(1), 46-56. https://link.springer.com/article/10.1007/BF00310881.

Harris N., Massey J., Inger S. 1993. The role of fluids in the formation of High Himalayan leucogranites. Geological Society, London, Special Publications, 74(1), 391-400. https://doi.org/10.1144/GSL.SP.1993.074.01.26 .

Hawkesworth C.J., Gallagher K., Hergt J.M., McDermott F. 1993. Mantle and slab contributions in arc magmas. Annual Review of Earth and Planetary Sciences, 21(1), 175-204. https://doi.org/10.1146/annurev.ea.21.050193.001135 .

Hurley P.M., Rand J.R., Pinson W.H., Fairbairn H.W., Almeida F.F.M., Melcher G.C., Cordani U.G., Kawashita K., VANDOROS, P. 1967. Test of Continental Drift by Comparison of Radiometric Ages: A pre-drift reconstruction shows matching geologic age provinces in West Africa and Northern Brazil. Science, 157(3788), 495-500. https://doi.org/10.1126/science.157.3788.495 .

Janoušek V., Farrow C.M., Erban V. 2006. Interpretation of whole-rock geochemical data in igneous geochemistry: introducing Geochemical Data Toolkit (GCDkit). Journal of Petrology, 47(6), 1255-1259. https://doi.org/10.1093/petrology/egl013 .

Jorge João X.S., Vale A.G., Lobato T.A.M. 1987. Altamira: folha SA.22-Y-D, Estado do Pará. Texto explicativo, escala 1:250.000. Programa Levantamentos Geológicos Básicos do Brasil (PLGB). Brasília, DNPM, CPRM, 31 p. Available online at: https://rigeo.cprm.gov.br/handle/doc/2973 / (accessed on 14 September 2022).

Jorge João X.S.; Silva Neto C.S. 1994. Metamorfismo e deformação. In: Oliveira J.R., Silva Neto C.S., Costa E.J.S. Serra Pelada: folha SB.22.X.C, Estado do Pará. Texto explicativo. Programa Levantamentos Geológicos Básicos do Brasil (PLGB), Brasília, CPRM, p. 77-86. Available online at: https://rigeo.cprm.gov.br/handle/doc/8327 / (accessed on 14 September 2022).

Jung S., Mezger K., Hoernes S. 2001. Trace element and isotopic (Sr, Nd, Pb, O) arguments for a mid-crustal origin of Pan-African garnet-bearing S-type granites from the Damara orogen (Namibia). Precambrian Research, 110(1-4), 325-355. https://doi.org/10.1016/S0301-9268(01)00175-9 .

Kemp A.I.S., Hawkesworth C.J. 2003. Granitic perspectives on the generation and secular evolution of the continental crust. In: Holland H.D., Turekian K.K. (eds.). Treatise on Geochemistry. Amsterdam, Elsevier, Pergamon, v. 3, p. 349-410.

King P.L., Chappell B.W., Allen C.M., White A.J.R. 2001. Are A-type granites the high-temperature felsic granites? Evidence from fractionated granites of the Wangrah Suite. Australian Journal of Earth Sciences, 48(4), 501-514. https://doi.org/10.1046/j.1440-0952.2001.00881.x .

King P.L., White A.J.R., Chappell B.W., Allen C.M. 1997. Characterization and origin of aluminous A-type granites from the Lachlan Fold Belt, southeastern Australia. Journal of petrology, 38(3), 371-391. https://doi.org/10.1093/petroj/38.3.371 .

Klein E.L., Rodrigues J.B., Lopes E.C., Soledade G.L. 2012. Diversity of Rhyacian granitoids in the basement of the Neoproterozoic-Early Cambrian Gurupi Belt, northern Brazil: Geochemistry, U–Pb zircon geochronology, and Nd isotope constraints on the Paleoproterozoic magmatic and crustal evolution. Precambrian Research, 220, 192-216. https://doi.org/10.1016/j.precamres.2012.08.007 .

Lameyre J., Bowden P. 1982. Plutonic rock types series: discrimination of various granitoid series and related rocks. Journal of Volcanology and Geothermal Research, 14(1-2), 169-186. https://doi.org/10.1016/0377-0273(82)90047-6 .

Landenberger B., Collins W.J. 1996. Derivation of A-type granites from a dehydrated charnockitic lower crust: evidence from the Chaelundi Complex, Eastern Australia. Journal of Petrology, 37(1), 145-170. https://doi.org/10.1093/petrology/37.1.145 .

Le Breton N., Thompson A.B. 1988. Fluid-absent (dehydration) melting of biotite in metapelites in the early stages of crustal anatexis. Contributions to Mineralogy and Petrology, 99(2), 226-237. http://dx.doi.org/10.1007/BF00371463 .

Le Maitre R.W., Streckeisen A., Zanettin B., Le Bas M.J., Bonin B., Bateman P., Bellieni G., Dudek A., Efremova S., Keller J., Lameyre J., Sabine P.A., Schmid R., Sorensen H., Woolley A.R. 2002. Igneous rocks: a classification and glossary of terms, 2nd. Edition, Cambridge, Cambridge University Press, 236 p.

Liégeois J.P., Claessens W., Camara D., Klerkx J. 1991. Short-lived Eburnian orogeny in southern Mali. Geology, tectonics, U-Pb and Rb-Sr geochronology. Precambrian Research, 50(1-2), 111-136. https://doi.org/10.1016/0301-9268(91)90050-K .

Loiselle M.C., Wones D.R. 1979. Characteristics and origin of anorogenic granites. Geological Society of America Abstracts with Programs 11(7), 468.

Macambira M.J.B., Silva D.C.C., Barros C.E.M., Scheller T. 2003. New isotope evidences confirming the existence of a Paleoproterozoic terrain in the region at the north of the Carajas Mineral Province. In: South American Symposium on Isotope Geology, 4, 205-208.

Macambira M.J.B., Vasquez M.L., Barros C.E.M. 2004. Investigação do limite Arqueano-Paleoproterozoico ao norte da Província de Carajás, Amazônia Oriental. In: Congresso Brasileiro de Geologia, 42. Available online at: http://www.sbgeo.org.br/home/pages/33 / (accessed on 14 September 2022).

Maniar P.D., Piccoli P.M. 1989. Tectonic discrimination of granitoids. Geological society of America bulletin, 101(5), 635-643. https://doi.org/10.1130/0016-7606(1989)101%3C0635:TDOG%3E2.3.CO;2 .

Martin H., Moyen J.F. 2002. Secular changes in tonalite-trondhjemite-granodiorite composition as markers of the progressive cooling of Earth. Geology, 30(4), 319-322. http://dx.doi.org/10.1130/0091-7613(2002)030%3C0319:SCITTG%3E2.0.CO;2 .

Martin H. 1994. The Archean grey gneisses and the genesis of continental crust. Developments in Precambrian geology, 11, 205-259. https://doi.org/10.1016/S0166-2635(08)70224-X .

Martin H., Smithies R.H., Rapp R., Moyen J.F., Champion D. 2005. An overview of adakite, tonalite–trondhjemite–granodiorite (TTG), and sanukitoid: relationships and some implications for crustal evolution. Lithos, 79(1-2), 1-24. https://doi.org/10.1016/j.lithos.2004.04.048 .

Martin R.F. 2006. A-type granites of crustal origin ultimately result from open-system fenitization-type reactions in an extensional environment. Lithos, 91(1-4), 125-136. http://dx.doi.org/10.1016/j.lithos.2006.03.012.

Martins H. 1987. Archaean and modern granitoids as indicators of changes in geodynamic processes. Rev. Bras. Geoc., 17(4), 360-365.

McDonough W.F., Sun S.S. 1995. The composition of the Earth. Chemical geology, 120(3-4), 223-253. http://dx.doi.org/10.1016/0009-2541(94)00140-4 .

Milési J.P., Ledru P., Feybesse J.L., Dommanget A., Marcoux E. 1992. Early Proterozoic ore deposits and tectonics of the Birimian orogenic belt, West Africa. Precambrian Research, 58(1-4), 305-344. https://doi.org/10.1016/0301-9268(92)90123-6 .

Motta J.G., Souza Filho C.R., Carranza E.J.M., Braitenberg C. 2019. Archean crust and metallogenic zones in the Amazonian Craton sensed by satellite gravity data. Scientific reports, 9(1), 1-10. Available online at: https://www.nature.com/articles/s41598-019-39171-9 / (accessed on 14 September 2022).

Nardi L.V., Bitencourt M.F. 2009. A-type granitic rocks in post-collisional settings in southernmost Brazil: their classification and relationship with tectonics and magmatic series. The Canadian Mineralogist, 47(6), 1493-1503. https://doi.org/10.3749/canmin.47.6.1493 .

Patiño Douce A.E.P., Johnston A.D. 1991. Phase equilibria and melt productivity in the pelitic system: implications for the origin of peraluminous granitoids and aluminous granulites. Contributions to Mineralogy and Petrology, 107(2), 202-218. https://doi.org/10.1007/BF00310707 .

Patiño Douce A.E.P. 1997. Generation of metaluminous A-type granites by low-pressure melting of calc-alkaline granitoids. Geology, 25(8), 743-746. https://doi.org/10.1130/0091-7613(1997)025%3C0743:GOMATG%3E2.3.CO;2 .

Patiño Douce A.E.P., Beard J.S. 1995. Dehydration melting of biotite gneiss and quartz amphibolite from 3 to 15 Kbar. Journal of Petrology, 36, 707-738. https://doi.org/10.1093/petrology/36.3.707 .

Pearce J.A., Peate D.W. 1995. Tectonic implications of the composition of volcanic arc magmas. Annual review of Earth and planetary sciences, 23, 251-286. https://doi.org/10.1146/annurev.ea.23.050195.001343.

Pearce J.A., Harris N.B.W., Tindle A.G. 1984. Trace element discrimination diagrams for the tectonic interpretation of granitic rocks. Journal of petrology, 25(4), 956-983. https://doi.org/10.1093/petrology/25.4.956 .

Pearce J. 1996. Sources and settings of granitic rocks. Episodes, 19(4), 120-125. https://doi.org/10.18814/epiiugs/1996/v19i4/005 .

Peccerillo A., Taylor S.R. 1976. Geochemistry of Eocene calc-alkaline volcanic rocks from the Kastamonu area, northern Turkey. Contributions to mineralogy and petrology, 58(1), 63-81. http://dx.doi.org/10.1007/BF00384745 .

Pehrsson S.J., Buchan K.L., Eglington B.M., Berman R.M., Rainbird R.H. 2014. Did plate tectonics shutdown in the Palaeoproterozoic? A view from the Siderian geologic record. Gondwana Research, 26(3-4), 803-815. http://dx.doi.org/10.1016/j.gr.2014.06.001 .

Pitcher W.S. 1987. Granites and yet more granites forty years on. Geologische Rundschau, 76(1), 51-79. http://dx.doi.org/10.1007/bf01820573 .

Rapp R.P., Watson E.B. 1995. Dehydration melting of metabasalt at 8–32 kbar: implications for continental growth and crust-mantle recycling. Journal of Petrology, 36(4), 891-931. https://doi.org/10.1093/petrology/36.4.891 .

Reddy S.M., Evans D.A.D. 2009. Palaeoproterozoic supercontinents and global evolution: correlations from core to atmosphere. Geological Society, London, Special Publications, 323(1), 1-26. https://doi.org/10.1144/SP323.1 .

Ricci P.S.F. 2006. Mineralogically bizarre charnockitoids of the Bacajá High-Grade Block (Pará): discharnockitized and reemplaced plutons mistakenly confused with granitoids crystallized at shallower crustal levels. Simpósio de Geologia da Amazônia, 9, 189-192. Available online at: https://www.sbg-no.org.br/ / (accessed on 14 September 2022).

Rollinson H.R. 1992. Another look at the constant sum problem in geochemistry. Mineralogical Magazine, 56(385), 469-475. http://dx.doi.org/10.1180/minmag.1992.056.385.03 .

Rollinson H.R. 1993. Using geochemical data: evaluation, presentation, interpretation. London, Routledge, 384 p. https://doi.org/10.4324/9781315845548 .

Rosa-Costa L.T., Chaves C.L., Klein E.L. 2014. Geologia e recursos minerais da Folha Rio Araguari – NA.22-Y-B, Estado do Amapa, Escala 1:250.00. Belém, CPRM, p. 159. Available online at: https://rigeo.cprm.gov.br/handle/doc/20623 / (accessed on 14 September 2022).

Salgado S.S., Caxito F.A., Silva R.C.F., Lana C. 2019. Provenance of the Buritirama Formation reveals the Paleoproterozoic assembly of the Bacajá and Carajás blocks (Amazon Craton) and the chronocorrelation of Mn-deposits in the Transamazonian/Birimian system of northern Brazil/West Africa. Journal of South American Earth Sciences, 96, 102364. https://doi.org/10.1016/j.jsames.2019.102364 .

Santos J.O.S. 2003. Geotectônica dos escudos das Guianas e Brasil-Central. In: Bizzi L.A., Schobbenhaus C., Vidotti R.M., Gonçalves J.H. (eds.). Geologia, Tectônica e Recursos Minerais do Brasil (texto, mapas & SIG). Brasília, CPRM, MME, p. 169-226.

Santos J.O.S., Hartmann L.A., Faria M.D., Riker S.R., Souza M.D., Almeida, M.E., McNaughton N.J. 2006. A compartimentação do Cráton Amazonas em províncias: avanços ocorridos no período 2000-2006. Simpósio de Geologia da Amazônia, 9, 156-159. Available online at: https://www.sbg-no.org.br/ / (accessed on 14 September 2022).

Santos T.J., Fetter A.H., Van Schmus W.R., Hackspacher P.C. 2009. Evidence for 2.35 to 2.30 Ga juvenile crustal growth in the northwest Borborema Province, NE Brazil. Geological Society, London, Special Publications, 323(1), 271-281. https://doi.org/10.1144/SP323.13 .

Santosh M., Shaji E., Tsunogae T., Mohan M.R., Satyanarayanan M., Horie K. 2013. Suprasubduction zone ophiolite from Agali hill: petrology, zircon SHRIMP U–Pb geochronology, geochemistry and implications for Neoarchean plate tectonics in southern India. Precambrian Research, 231, 301-324. https://doi.org/10.1016/j.precamres.2013.04.003

Saunders A.D., Norry M.J., Tarney J. 1991. Fluid influence on the trace element compositions of subduction zone magmas. Philosophical Transactions of the Royal Society of London. Series A: Physical and Engineering Sciences, 335(1638), 377-392. https://doi.org/10.1098/rsta.1991.0053 .

Schandl E.S., Gorton M.P. 2002. Application of high field strength elements to discriminate tectonic settings in VMS environments. Economic geology, 97(3), 629-642. https://doi.org/10.2113/gsecongeo.97.3.629 .

Skjerlie K.P., Johnston A.D. 1992. Vapor-absent melting at 10 kbar of a biotite-and amphibole-bearing tonalitic gneiss: implications for the generation of A-type granites. Geology, 20(3), 263-266. https://doi.org/10.1130/0091-7613(1992)020%3C0263:VAMAKO%3E2.3.CO;2 .

Streckeisen A. 1976. To each plutonic rock its proper name. Earth-science reviews, 12 (1), 1-33. https://doi.org/10.1016/0012-8252(76)90052-0 .

Swain G., Woodhouse A., Hand M., Barovich K., Schwarz M., Fanning C.M. 2005. Provenance and tectonic development of the late Archaean Gawler Craton, Australia; U–Pb zircon, geochemical and Sm–Nd isotopic implications. Precambrian Research, 141(3-4), 106-136. http://dx.doi.org/10.1016/j.precamres.2005.08.004 .

Sylvester P.J. 1989. Post-collisional alkaline granites. The Journal of Geology, 97(3), 261-280. https://doi.org/10.1086/629302 .

Tassinari C.C.G., Bettencourt J.S., Geraldes M.C., Macambira M.J.B., Lafon J.M. 2000. The Amazonian Craton. Cordani U.G., Milani E.J., Thomaz Filho A., Campos D.A. Tectonic Evolution of South America. Rio de Janeiro, 31st International Geological Congress, p. 41-95. Available online at: https://rigeo.cprm.gov.br/handle/doc/19419 / (accessed on 14 September 2022).

Tassinari C.C., Macambira M.J. 1999. Geochronological provinces of the Amazonian Craton. Episodes Journal of International Geoscience, 22(3), 174-182. https://doi.org/10.18814/epiiugs/1999/v22i3/004.

Tassinari C.C.G., Macambira M.J.B. 2004. A evolução tectônica do Cráton Amazônico. Mantesso-Neto V., Bartorelli A., Carneiro C.D.R., Brito-Neves B.B. Geologia do continente sul-americano: evolução da obra de Fernando Flávio Marques de Almeida. São Paulo, Beca, p. 471-485. Available online at: https://geologia.ufc.br/wp-content/uploads/2016/02/geologia-do-continente.pdf / (accessed on 14 September 2022).

Toledo P.I.F., Moreto C.P.N., Xavier R.P., Gao J., Melo G.H.C. 2019. Multistage Evolution of the Neoarchean (ca. 2.7 Ga) Igarapé Cinzento (GT-46) Iron Oxide Copper-Gold Deposit, Cinzento Shear Zone, Carajás Province, Brazil. Economic Geology, 114(1), 1-34. https://doi.org/10.5382/econgeo.2019.4617 .

Turner S., Sandiford M., Foden J. 1992. Some geodynamic and compositional constraints on" postorogenic" magmatism. Geology, 20(10), 931-934. http://dx.doi.org/10.1130/0091-7613(1992)020%3C0931:SGACCO%3E2.3.CO;2 .

Vasquez M.L. 2006. Geocronologia em zircão, monazita e granada e isotópos de Nd das associações litológicas da porção oeste do domínio Bacajá: evolução crustal da porção meridional da província Maroni-itacaiúnas-sudeste do cráton Amazônico. PhD Thesis, Programa de Pós-Graduação em Geologia e Geoquímica, Centro de Geociências, Universidade Federal do Pará, Belém, 212 f. Available online at: http://repositorio.ufpa.br:8080/jspui/handle/2011/8285 / (accessed on 14 September 2022).

Vasquez M.L., Macambira M.J.B., Armstrong R.A. 2008. Zircon geochronology of granitoids from the western Bacajá domain, southeastern Amazonian craton, Brazil: Neoarchean to Orosirian evolution. Precambrian Research, 161(3-4), 279-302. https://doi.org/10.1016/j.precamres.2007.09.001 .

Vasquez M.L., Macambira M.J.B., Galarza M.A. 2005. Granitóides transamazônicos da Região Iriri-Xingu, Pará-Novos dados geológicos e geocronológicos. In: Souza V.S., Horbe A.M.C. Contribuições a Geologia da Amazônia, Sociedade Brasileira de Geologia, v. 4, p. 16-31.

Vasquez M.L., Macambira M.J., Armstrong R.A. 2006. SHRIMP ages for granitoids from Bacajá domain, southeastern Amazonian craton, Brazil; new evidence of Siderian accretion. In: Symposium on South American Isotope Geology, 5, 250-253.

Vasquez M. L., Rosa-Costa L.T. 2008. Geologia e recursos minerais do estado do Pará: texto explicativo dos mapas Geológico e Tectônico e de Recursos Minerais do Estado do Pará. Belém, CPRM, 328 p. Available online at: https://rigeo.cprm.gov.br/handle/doc/10443 / (accessed on 28 September 2022).

Vendemiatto M.A., Enzweiler J. 2001. Routine control of accuracy in silicate rock analysis by X-ray fluorescence spectrometry. Geostandards Newsletter, 25(2-3), 283-291. https://doi.org/10.1111/j.1751-908X.2001.tb00604.x .

Vianna S.Q., Lafon J.M., Neto J.M.M., Silva D.P.B., Mesquita Barros C.E. 2020. U–Pb geochronology, Nd–Hf isotopes, and geochemistry of Rhyacian granitoids from the Paleoproterozoic Lourenço domain (Brazil), southeastern Guiana Shield. Journal of South American Earth Sciences, 104, 102937. https://doi.org/10.1016/j.jsames.2020.102937 .

Vianna S.Q., Lafon J.M., Neto J.M.M., Silva D.P.B., Mesquita Barros C.E. 2020. U–Pb geochronology, Nd–Hf isotopes, and geochemistry of Rhyacian granitoids from the Paleoproterozoic Lourenço domain (Brazil), southeastern Guiana Shield. Journal of South American Earth Sciences, 104, 102937. https://doi.org/10.1016/j.jsames.2020.102937 .

Weller O.M., ST-Onge M.R. 2017. Record of modern-style plate tectonics in the Palaeoproterozoic Trans-Hudson orogen. Nature Geoscience, 10(4), 305-311. https://ui.adsabs.harvard.edu/link_gateway/2017NatGe..10..305W/doi:10.1038/ngeo2904 .

White A.J.R. 1979. Sources of granite magmas. Geol. Soc. Amer. Abstr. With Prog. 11(7), 539.

Whitney D.L., Evans B.W. 2010. Abbreviations for names of rock-forming minerals. American mineralogist, 95(1), 185-187.

Wiedenbeck M.A.P.C., Alle P., Corfu F., Griffin W.L., Meier M., Oberli, F., Von Quadt A., Roddick J.C., SPIEGEL, W. 1995. Three natural zircon standards for U-Th-Pb, Lu-Hf, trace element and REE analyses. Geostandards newsletter, 19(1), 1-23. https://doi.org/10.1111/j.1751-908X.1995.tb00147.x .

Williamson B.J., Shaw A., Downes H., Thirlwall M.F. 1996. Geochemical constraints on the genesis of Hercynian two-mica leucogranites from the Massif Central, France. Chemical Geology, 127(1-3), 25-42. https://doi.org/10.1016/0009-2541(95)00105-0 .

Wu F-Y., Jahn B-M., Wilde S.A., Lo C-H., YUI, T-F., LIN, Q., Ge W-C., SUN, D-Y. 2003. Highly fractionated I-type granites in NE China (II): isotopic geochemistry and implications for crustal growth in the Phanerozoic. Lithos, 67(3-4), 191-204. https://doi.org/10.1016/S0024-4937(03)00015-X .

Wyllie P.J. 1983. Experimental and thermal constraints on the deep-seated parentage of some granitoid magmas in subduction zones. In: Atherton M.P., Gribble C.D. (eds) Migmatites, Melting and Metamorphism. Nantwich, Shiva, p. 37-51.

Yang, J. H., Wu, F. Y., Chung, S. L., Wilde, S. A., Chu, M. F., Lo, C. H., Song, B. 2005. Petrogenesis of Early Cretaceous intrusions in the Sulu ultrahigh-pressure orogenic belt, east China and their relationship to lithospheric thinning. Chemical Geology, 222(3-4), 200-231. https://doi.org/10.1016/j.chemgeo.2005.07.006.

Zartman R.E., Doe B.R. 1981. Plumbotectonics - the model. Tectonophysics, 75(1-2), 135-162. https://doi.org/10.1016/0040-1951(81)90213-4 .

Zhang L., Ma C-Q, Wang L-X, She Z-B, Wang S-M. 2011. Discovery of Paleoproterozoic rapakivi granite on the northern margin of the Yangtze block and its geological significance. Chinese Science Bulletin, 56(3), 306-318.

Zhao G., Cawood P.A., Wilde S.A., Sun M. 2002. Review of global 2.1–1.8 Ga orogens: Implications for a pre-Rodinia supercontinent: Earth-Science Reviews, 59, 125–162. http://dx.doi.org/10.1016/S0012-8252(02)00073-9 .

Zhu D-C., Wang Q., Zhao Z-D., Chung S-L., Cawood P.A., Niu Y-L., Liu S-A., Wu F-Y., Mo X-X. 2015. Magmatic record of India-Asia collision. Sci. Rep. 5, 1428. https://doi.org/10.1038/srep14289.